Flow, Turbulence and Combustion (2019) 103:913–941
https://doi.org/10.1007/s10494-019-00035-x

SI: THMT-2018

Propagation of Spherically Expanding Turbulent Flames into Fuel Droplet-Mists

Gulcan Ozel Erol[1] · Josef Hasslberger[2] · Markus Klein[2] · Nilanjan Chakraborty[1]

Received: 15 February 2019 / Accepted: 9 May 2019 / Published online: 12 June 2019
© Springer Nature B.V. 2019

Abstract

The effects of droplet diameter and the overall (liquid+gas) equivalence ratio on flame topology and propagation statistics in spherically expanding turbulent n-heptane spray flames have been analysed based on three-dimensional Direct Numerical Simulations (DNS) data. It has been found that the range of both mean and Gauss curvatures of the flame surface, and the probability of finding saddle topologies increase with increasing droplet diameter and overall equivalence ratio. The presence of droplets affects the displacement speed and consumption speed statistics principally through the reaction rate of the mixture composition in the reaction zone. The magnitudes of the components of density-weighted displacement speed arising from mixture inhomogeneity and droplet evaporation remain small in comparison to the magnitudes of the reaction rate and molecular diffusion rate components. The presence of large droplets decreases the mean density-weighted displacement speed S_d^* and increases the probability of finding negative S_d^* values, except for overall fuel-lean equivalence ratios. The mean consumption speed shows an increasing trend with increasing droplet diameter for fuel-lean overall equivalence ratios, whereas the mean consumption speed decreases with increasing droplet diameter for overall stoichiometric and fuel-rich mixtures. The mean consumption speed remains greater than the mean density-weighted displacement speed for all cases considered here. An alternative flame speed, which represents the growth rate of the flame surface area, has been found to provide an approximate measure of mean consumption flame speed. By contrast, an alternative flame speed, which represents the growth rate of burned gas volume, has been found to approximate the mean density-weighted displacement speed for large droplets in the case of stoichiometric and fuel-rich overall equivalence ratios.

Keywords Droplet combustion · Spherically expanding flame · Displacement speed · Consumption speed · Direct numerical simulations

✉ Gulcan Ozel Erol
G.Ozel-Erol2@newcastle.ac.uk

[1] School of Engineering, Newcastle University, Newcastle-Upon-Tyne NE17RU, UK

[2] Bundeswehr University Munich, Werner-Heisenberg-Weg 39, 85577 Neubiberg, Germany

1 Introduction

The propagation of statistically spherical flames in droplet-laden mixtures plays an important role in combustion processes in automotive engines, gas turbines, and accidental explosions. The spherically expanding flames represent a convenient canonical configuration for experimental [1–16] and numerical [9, 10, 17–37] investigations. However, most of the existing analyses on spherically expanding flames have been carried out for turbulent premixed flames [2–10, 12–34, 36] and only a limited number of analyses [1, 11, 35, 37] concentrated on propagation of spherically expanding flames in droplet-laden mixtures in spite of its importance in several engineering applications. To address this gap in the existing literature, the flame propagation statistics of spherically expanding flames in turbulent droplet-laden mixtures have been analysed in this paper.

The local flame propagation can be characterised with the help of different flame speeds, which focus on different aspects of the underlying combustion physics. The displacement speed S_d and consumption speed S_c are two widely used flame speeds, which are often used to identify the flame propagation characteristics [24–27, 38–42]. The displacement speed S_d indicates the speed with which the flame surface moves normal to itself with respect to an initially coincident material surface and is dependent on both chemical reaction rate and molecular diffusion rate within the flame [24–27, 38]. By contrast, the consumption speed S_c is related to the integrated reaction rate in the flame normal direction [38–42]. However, experimental evaluation of local displacement and consumption speeds (i.e. S_d and S_c) is a challenging task for three-dimensional flame surfaces under turbulent conditions. The challenges associated with precise evaluation of flame speed were discussed by Abdel-Gayed *et al.* [2] for statistically spherical turbulent premixed flames. Nwagwe *et al.* [6] analysed the growth of the burned gas kernel by considering a mean radius of the flame for the purpose of an effective comparison between numerical and experimental data. Considerable uncertainty still exists about the experimental evaluations of flame speeds for spherically expanding turbulent flames. Therefore a number of different experimental approaches [15, 41, 42] have been suggested for the flame speed evaluations, which need further validation.

The advances in high performance computing have enabled Direct Numerical Simulations (DNS) of turbulent reacting flows, which offer three-dimensional spatially and temporally resolved information for reliable evaluations of S_d and S_c. Poinsot *et al.* [38] used two-dimensional laminar simulations of Bunsen burner premixed flames to compare the statistics of S_d and S_c, and revealed that flame curvature significantly influences the statistics of displacement speed in turbulent premixed flames [24–27, 43–52], whereas the consumption speed remains unaffected by flame curvature for unity Lewis number flames. These findings have subsequently been verified for turbulent statistically planar premixed flames [39, 40]. The strain rate and curvature dependences of displacement speed for statistically planar premixed turbulent flames have been investigated in detail based on both detailed chemistry DNS [43–45, 48, 49, 51] and simple chemistry DNS [24–27, 46, 47, 50, 52] data and it has been found that local displacement speed shows negative correlation with curvature in the absence of significant differential diffusion of heat and mass. The combined reaction and normal diffusion components of displacement speed S_d have been found to be negatively correlated with tangential strain rate a_T, whereas the tangential diffusion component of S_d correlates positively with a_T [24, 25, 27, 46, 47, 50]. These two correlations ultimately determine the tangential strain rate dependence of displacement speed in statistically planar premixed turbulent flames [24, 25, 27, 46, 47, 50]. The statistics of displacement speed in statistically

spherical turbulent premixed flames can be considerably different from the corresponding statistically planar premixed flames [25, 27, 30]. These differences originate because of the strain rate and curvature dependences of reactive scalar gradient in the presence of mean positive curvature in spherically expanding flames. The differences in flame speeds and their curvature and stretch rate dependences between the statistically planar and spherical flames also depend on the mean flame radius [25, 27, 30]. Similarly, it has also been reported by Mizutani and Nishimoto [53] that propagation of statistically spherical flames expanding in droplet-laden mixtures can be considerably different from statistically planar spray flames.

In addition to chemical reaction rate and molecular diffusion rate, turbulent flame propagation in droplet-laden mixtures is affected by the additional physical mechanisms arising from evaporation and partial mixing of evaporated fuel with the surrounding air. Flame structure and flame propagation characteristics have been analytically [54–56], experimentally [57–59] and numerically [60–69] investigated for statistically planar and jet spray flames. Moreover, the ignition performance of droplet-laden mixtures has been reported for a range of overall equivalence ratios and droplet diameters using the carrier phase DNS [70–75]. Wacks *et al.* [69] and Wacks and Chakraborty [67] carried out three-dimensional DNS with a modified single step Arrhenius chemical mechanism to analyse the influences of droplet diameter and overall (i.e. gaseous+liquid) equivalence ratio on the flame speed statistics for statistically planar flames propagating in droplet-laden mixtures. It has been demonstrated by Wacks *et al.* [69] and Wacks and Chakraborty [67] that the magnitudes of the components of density-weighted displacement speed due to mixture inhomogeneity and droplet evaporation are small compared to the reaction and normal diffusion components. However, the analyses of Wacks *et al.* [69] and Wacks and Chakraborty [67] were conducted for statistically planar flames and thus it needs to be assessed if the previously drawn conclusions for statistically planar flames are also valid for spherically expanding flames.

Recently, Ozel-Erol *et al.* [35, 37] investigated the combustion characteristics and flame structure of spherically expanding spray flames for a range of different droplet diameters, overall equivalence ratios and turbulence intensities using three-dimensional DNS with a modified single-step chemical mechanism. The effects of droplet diameter, overall equivalence ratio and turbulence intensity on droplet-induced flame wrinkling, flame surface area and the volume of burned gas for spherically expanding turbulent flames propagating into mono-sized droplets, according to the DNS analysis by Ozel-Erol *et al.* [35, 37], have been found to be qualitatively consistent with the experimental results by Hayashi *et al.* [1] and Lawes and Saat [11]. The DNS database by Ozel-Erol *et al.* [37] has been utilised in this paper to analyse the statistical behaviours of displacement speed S_d and consumption speed S_c in spherically expanding flames propagating into turbulent mono-sized droplet-laden mixtures for different initial droplet diameters and overall equivalence ratios (i.e. $\phi_{ov} = 0.8$, 1.0 and 1.2). In this respect, the main objectives of the current analysis are:

(a) to demonstrate and explain the effects of initial droplet diameter and the overall equivalence ratio on displacement speed and consumption speed statistics in spherically expanding turbulent flames propagating into initially mono-sized droplet-laden mixtures,
(b) to relate displacement and consumption speeds with the rates of flame area generation and the burned gas volume in spherically expanding turbulent spray flames.

The rest of this paper is organised as follows. The next two sections will focus upon the mathematical background and numerical implementation pertaining to this analysis. This will be followed up by the presentation of the results and their discussion. The summary of the main findings along with the conclusions are provided in the final section of this paper.

2 Mathematical Background

In the present analysis, a modified single-step irreversible chemical reaction with an Arrhenius reaction rate expression [76] has been adopted for the purpose of computational efficiency in the interests of a detailed parametric analysis. The activation energy and heat of combustion are calculated depending on the gaseous equivalence ratio, ϕ_g following the model proposed by Tarrazo *et al*. [76] which can capture main flame features (i.e. accurate equivalence ratio ϕ_g dependence of the unstrained laminar burning velocity $S_{b(\phi_g)}$ and adiabatic flame temperature $T_{ad(\phi_g)}$) for hydrocarbon fuels. Interested readers are referred to Malkeson and Chakraborty [77] for further discussion on the variation of the laminar burning velocity $S_{b(\phi_g)}$ with equivalence ratio ϕ_g for hydrocarbon fuels. Swaminathan and Bray [78] demonstrated that ϕ_g dependence of the normalised laminar burning velocity $S_{b(\phi_g)}/\left\{S_{b(\phi_g)}\right\}_{max}$ does not change significantly for different hydrocarbon fuels. It has also been found that the variations of $S_{b(\phi_g)}/\left\{S_{b(\phi_g)}\right\}_{max}$ and $T_{ad(\phi_g)}$ with ϕ_g for the present thermo-chemistry remain in good agreement with previous experimental observations [79] and the results obtained using a detailed chemical mechanism [80]. It is worth noting that several previous computational analyses [63–65, 70–73] on combustion of droplet-laden mixtures including ignition and extinction events in turbulent spray flames utilised single step chemistry in the past and provided important physical insights, which were consistent with experimental findings. Furthermore, flame propagation statistics obtained from modified single step chemical mechanism [67, 69] for droplet-laden mixtures have been found to be qualitatively consistent with those obtained from detailed chemistry simulations [74, 75].

The Lewis numbers of all species are assumed to be unity and all species in the gaseous phase are taken to be perfect gases. Standard values have been considered for the ratio of specific heats ($\gamma = C_p^g/C_v^g = 1.4$, where C_p^g and C_v^g are the gaseous specific heats at constant pressure and volume, respectively) and Prandtl number ($Pr = \mu C_p^g/\lambda = 0.7$ where μ, is the dynamic viscosity and λ is the thermal conductivity of the gaseous phase).

Standard compressible Navier-Stokes equations for reactive flows for the carrier gaseous phase are solved in an Eulerian frame of reference, and these equations can be given by the following generic form [60, 67–69, 72, 73]:

$$\frac{\partial(\rho\psi)}{\partial t} + \frac{\partial\left(\rho u_j \psi\right)}{\partial x_j} = \frac{\partial}{\partial x_j}\left(\Gamma_\psi \frac{\partial \psi_1}{\partial x_j}\right) + \dot{w}_\psi + \dot{S}_g + \dot{S}_\psi \tag{1}$$

Here, ρ stands for the gas density, u_i is the ith component of fluid velocity, $\psi = \{1, u_i, e, Y_F, Y_O\}$ and $\psi_1 = \left\{1, u_i, \hat{T}, Y_F, Y_O\right\}$ for the conservation equations of mass, momentum, energy, and mass fractions, respectively and the diffusion coefficients are given by: $\Gamma_\psi = \rho\nu/\sigma_\psi$ for $\psi = \{1, u_i, Y_F, Y_O\}$ and $\Gamma_\psi = \lambda$ for $\psi = e$, respectively. Here, Y_F and Y_O are the fuel and oxygen mass fractions, $\hat{T}$ denotes the instantaneous dimensional temperature and $e = C_v^g\left(\hat{T} - T_{ref}\right) + u_k u_k/2$ represents the specific total internal energy. The $\dot{w}_\psi$ term arises due to chemical reaction rate, $\dot{S}_g$ is an appropriate source/sink term in the gaseous phase and $\dot{S}_\psi$ is the appropriate source term due to coupling between Eulerian and Lagrangian phases, which is tri-linearly interpolated from the droplet's sub-grid position, $\vec{x}_d$, to the eight surrounding nodes. Other variables are ν, kinematic viscosity, and σ_ψ, an appropriate Schmidt number corresponding to ψ. The droplet source term for

any variable ψ is expressed as [60, 67–69, 72, 73]: $\dot{S}_\psi = -(1/V)\sum_d d(m_d\psi_d)/dt$ where, V is the cell volume, $m_d = \rho_d(1/6)\pi a_d^3$ is the droplet mass. A Lagrangian approach is adopted to solve the quantities transported for each droplet, which are position, $\vec{x}_d$, velocity, $\vec{u}_d$, diameter, a_d and temperature, T_d of the individual droplets. The transport equations for these quantities are [60, 67–69, 72, 73]:

$$\frac{d\vec{x}_d}{dt} = \vec{u}_d; \frac{d\vec{u}_d}{dt} = \frac{\vec{u}(\vec{x}_d,t) - \vec{u}_d}{\tau_d^u}; \frac{da_d^2}{dt} = -\frac{a_d^2}{\tau_d^p}; \frac{dT_d}{dt} = \frac{\hat{T}(\vec{x}_d,t) - T_d - B_d L_v/C_P^g}{\tau_d^T} \tag{2}$$

where L_v is the latent heat of vaporisation, and τ_d^u, τ_d^p and τ_d^T are relaxation timescales for velocity, droplet diameter and temperature, respectively, which are defined as [60, 67–69, 72, 73]:

$$\tau_d^u = \frac{\rho_d a_d^2}{18 C_u \mu}; \tau_d^p = \frac{\rho_d a_d^2}{4\mu}\frac{Sc}{Sh_c}\frac{1}{\ln(1+B_d)}; \tau_d^T = \frac{\rho_d a_d^2}{6\mu}\frac{Pr}{Nu_c}\frac{B_d}{\ln(1+B_d)}\frac{C_p^L}{C_p^g} \tag{3}$$

where ρ_d is the droplet density, Sc is the Schmidt number, C_p^L is the specific heat for the liquid phase, $C_u = 1 + Re_d^{2/3}/6$ with the droplet Reynolds number Re_d, B_d is the Spalding number, Sh_c is the corrected Sherwood number, Nu_c is the corrected Nusselt number and the aforementioned non-dimensional numbers are defined as [60, 67–69, 72, 73]:

$$Re_d = \frac{\rho|\vec{u}(\vec{x}_d,t) - \vec{u}_d|a_d}{\mu}; B_d = \frac{Y_F^s - Y_F(\vec{x}_d,t)}{1 - Y_F^s}; \tag{4}$$
$$Sh_c = Nu_c = 2 + \frac{0.555 Re_d Sc}{\left(1.232 + Re_d Sc^{4/3}\right)^{1/2}}$$

Here, Y_F^s denotes the value of Y_F at the surface of the droplet which together with the partial pressure of the fuel vapour on the droplet surface p_F^s are expressed as [61, 68–70, 73, 74]:

$$p_F^s = p_{ref}\exp\left(L_v\left[\frac{1}{RT_{ref}^s} - \frac{1}{RT_d^s}\right]\right); Y_F^s = \left(1 + \frac{W_{air}}{W_F}\left[\frac{p(\vec{x}_d,t)}{p_F^s} - 1\right]\right)^{-1} \tag{5}$$

In Eq. 5, R is the universal gas constant, T_{ref}^s denotes the boiling point of the fuel at pressure p_{ref} and T_d^s is assumed to be T_d, and W_{air} and W_F are the molecular weights of air and fuel, respectively. More information on the mathematical framework are available elsewhere [60, 67–69, 72, 73] and interested readers are referred to Ozel-Erol et al. [35, 37] for further information.

A reaction progress variable, c based on oxygen mass fraction, Y_O and mixture fraction, $\xi = (Y_F - Y_O/s + Y_{O\infty}/s)/(Y_{F\infty} + Y_{O\infty}/s)$ can be defined as [67–69, 73]:

$$c = \frac{(1-\xi)Y_{O\infty} - Y_O}{(1-\xi)Y_{O\infty} - \max(0, \{\xi_{st} - \xi\}/\xi_{st})Y_{O\infty}} \tag{6}$$

where $Y_{O\infty} = 0.233$ is the oxygen mass fraction in air and $Y_{F\infty} = 1.0$ is the fuel mass fraction in the pure fuel stream. Considering n-heptane, C_7H_{16} as the fuel in the analysis, the stoichiometric mass ratio of oxidiser to fuel turns out to be $s = 3.52$ and $Y_{Fst} = \xi_{st} = 0.0621$ represents the corresponding stoichiometric fuel mass fraction and mixture fraction, respectively.

The transport equation of the reaction progress variable, c can be obtained by using the transport equations for oxygen mass fraction, Y_O and mixture fraction, ξ as [67–69]:

$$\rho\frac{\partial c}{\partial t}+\rho u_j\frac{\partial c}{\partial x_j}=\frac{\partial}{\partial x_j}\left(\rho D\frac{\partial c}{\partial x_j}\right)+\dot{w}_c+\dot{S}_{liq,c}+\dot{A}_c \tag{7}$$

In Eq. 7, D is the molecular diffusivity, $\dot{w}_c$ indicates the reaction rate of reaction progress variable, $\dot{S}_{liq,c}$ represents the source/sink term arising due to droplet evaporation and $\dot{A}_c$ is the cross-scalar dissipation term arising due to mixture inhomogeneity. The molecular diffusion term can be rewritten by splitting it into normal and tangential components as [45]: $\partial(\rho D\partial c/\partial x_j)/\partial x_j=\partial(\rho D\partial c/\partial x_N)/\partial x_N+2\rho D\kappa_m\partial c/\partial x_N$ where $\kappa_m=0.5(\partial N_i/\partial x_i)$ is the local mean curvature and N_j is the j^{th} component of the flame normal vector which can be defined as $N_j=-(\partial c/\partial x_j)/|\nabla c|$. According to the current convention, the flame normal vector points towards the reactants, whereas the flame surface, which is convex (concave) to the reactants, has a positive (negative) curvature.

The reaction rate of the reaction progress variable $\dot{w}_c$ can be expressed as [67–69]:

$$\dot{w}_c=-\xi_{st}\dot{w}_o/[Y_{O\infty}\xi(1-\xi_{st})]\text{ for }\xi\le\xi_{st};\ \dot{w}_c=-\dot{w}_o/[Y_{O\infty}(1-\xi)]\text{ for }\xi>\xi_{st} \tag{8}$$

The terms associated with droplet evaporation $\dot{S}_{liq,c}$ and mixture inhomogeneity $\dot{A}_c$ are given as [67–69]:

$$\dot{S}_{liq,c}=\begin{cases}-\dfrac{\xi_{st}}{Y_{O\infty}\xi^2(1-\xi_{st})}\cdot\left[\xi\dot{S}_O+(Y_{O\infty}-Y_O)\dot{S}_\xi\right] & \text{for }\xi\le\xi_{st};\\ -\dfrac{1}{Y_{O\infty}(1-\xi)^2}\cdot\left[(1-\xi)\dot{S}_O+Y_O\dot{S}_\xi\right] & \text{for }\xi>\xi_{st}\end{cases} \tag{9}$$

$$\dot{A}_c=\begin{cases}2\rho D\nabla\xi\cdot\nabla c/\xi & \text{for }\xi\le\xi_{st};\\ -2\rho D\nabla\xi\cdot\nabla c/(1-\xi) & \text{for }\xi>\xi_{st}\end{cases} \tag{10}$$

where $\dot{w}_o$ is the reaction rate of oxidiser, $\dot{S}_\xi=(\dot{S}_F-\dot{S}_O/s)/(Y_{F\infty}+Y_{O\infty}/s)$ is the droplet source/sink term in the mixture fraction transport equation, $\dot{S}_F=\Gamma_m(1-Y_F)$ and $\dot{S}_O=-\Gamma_m Y_O$ are the droplet source/sink terms in the mass fraction transport equations for fuel and oxygen, respectively and Γ_m is the source term in the mass conservation equation due to evaporation.

Alternatively, Eq. 7 can be rearranged in the kinetic form for a given c isosurface as [24–27, 43–52, 67–69]:

$$\frac{\partial c}{\partial t}+u_j\frac{\partial c}{\partial x_j}=S_d|\nabla c| \tag{11}$$

where S_d represents the displacement speed, which can be expressed as [67–69]:

$$S_d=\left[\frac{\nabla\cdot(\rho D\nabla c)+\dot{w}_c+\dot{S}_{liq,c}+\dot{A}_c]}{\rho|\nabla c|}=S_n+S_t+S_r+S_z+S_s\right. \tag{12}$$

where S_n, S_t, S_r are the normal diffusion, tangential diffusion, reaction components and S_z and S_s are the contributions associated with the cross-scalar dissipation term and droplet evaporation, respectively, which can be expressed as [67–69]:

$$S_n = \frac{\vec{N}\cdot\nabla\left(\rho D\vec{N}\cdot\nabla c\right)}{\rho|\nabla c|}; S_t = -2D\kappa_m; S_r = \frac{\dot{w}_c}{\rho|\nabla c|}; S_z = \frac{\dot{A}_c}{\rho|\nabla c|}; S_s = \frac{\dot{S}_{liq,c}}{\rho|\nabla c|} \quad (13)$$

It can be seen from Eqs. 12 and 13 that a change in density ρ can affect the displacement speed S_d and its components (i.e. S_n, S_t, S_r, S_z, S_s). Thus, it is worthwhile to consider density-weighted displacement speed $S_d^* = \rho S_d/\rho_0$ and its components: $S_r^* = \rho S_r/\rho_0$, $S_n^* = \rho S_n/\rho_0$, $S_t^* = \rho S_t/\rho_0$, $S_z^* = \rho S_z/\rho_0$ and $S_s^* = \rho S_s/\rho_0$ where ρ_0 is the unburned gas density. Moreover, ρS_d is often used for modelling purposes [81, 82] and thus it is useful to consider S_d^* instead of S_d. The local consumption speed S_c can be defined as [38–40]:

$$S_c = \rho_0^{-1}\int \dot{w}_c\, dn \quad (14)$$

where dn is the elemental distance in the local flame normal direction. The statistical behaviours of S_c and S_d^* and its components (i.e. S_r^*, S_n^*, S_t^*, S_z^* and S_s^*) and their curvature and strain rate dependences will be analysed in Section 4.

3 Numerical Implementation

The standard conservation equations of mass, momentum, energy and species of the gaseous phase in non-dimensional form are solved using a three-dimensional compressible DNS code SENGA [67–69, 71–75]. The spatial derivatives are evaluated using a 10th order central difference scheme for the internal grid points, but the order of differentiation gradually decreases to a one-sided 2nd order scheme at the non-periodic boundaries. The time advancement is conducted using an explicit low-storage 3rd order Runge-Kutta scheme [83]. Partially non-reflecting boundary conditions are assumed for all directions of the cubic domain of size $84.49\delta_z \times 84.49\delta_z \times 84.49\delta_z$ where $\delta_z = \alpha_{T0}/S_{b\left(\phi_g=1\right)}$ is the Zel'dovich flame thickness of the stoichiometric mixture with α_{T0} and $S_{b\left(\phi_g=1\right)}$ being the thermal diffusivity in the unburned gas and unstrained laminar burning velocity for the stoichiometric mixture, respectively. The partially non-reflecting boundary conditions are specified using the Navier-Stokes Characteristic Boundary Conditions (NSCBC) technique [84]. The simulation domain is discretised by a uniform Cartesian grid of $(512)^3$, which ensures about 10 grid points within the thermal flame thickness of the stoichiometric mixture $\delta_{st} = \left(T_{ad\left(\phi_g=1\right)} - T_0\right)/\max|\nabla T|_L$, where $T_{ad\left(\phi_g=1\right)}$ is the adiabatic flame temperature for the stoichiometric mixture and T_0 is the unburned gas temperature. A commercial software COSILAB [85] is used to generate the initial reacting flow field following Neophytou and Mastorakos [86] for three different initial values of droplet diameter a_d (i.e. $a_d/\delta_{st} = 0.04$, 0.05 and 0.06) and overall equivalence ratios ϕ_{ov} (i.e. $\phi_{ov} = 0.8$, 1.0 and 1.2) as described in a previous study by Ozel-Erol *et al.* [37]. A perfectly spherical kernel flame is allowed to propagate from the centre of the cubic domain until the radius of the fully burned gas region (i.e. the region corresponding to reaction progress variable c values greater than 0.99) r_0 reaches $2\delta_{st}$ (i.e. $r_0/\delta_{st} = 2.0$), then an incompressible homogeneous isotropic velocity field [87] is superimposed on the laminar spherical flames. It is important to note that the energy content for a premixed spherical flame with radius $r_0 = 2\delta_{st}$ is different from a spherical droplet flame with the same burned gas radius (i.e. $c \geq 0.99$) for a given equivalence ratio. However, the same initial burned gas (i.e. $c \geq 0.99$) radius (i.e. $r_0/\delta_{st} = 2.0$) has been considered here for the purpose of comparison. The unburned gas temperature T_0 is

assumed to be 300 K and this implies a heat release parameter $\tau = \left(T_{ad\left(\phi_g=1\right)}-T_0\right)/T_0$ of 6.54. The turbulent flame simulations are carried out under decaying turbulence for an initial value of normalised root-mean-square (rms) turbulent velocities of $u'/S_{b\left(\phi_g=1\right)} = 4.0$ with a non-dimensional longitudinal integral length-scale of L_{11}/δ_{st}=2.5, and have been continued for $2.52\alpha_{T0}/S^2_{b\left(\phi_g=1\right)}$, which corresponds to about 2.0 initial eddy turnover times (i.e. $2L_{11}/u'$). All cases considered here are subjected to same initial turbulence, generated using a pseudo spectral method [87], as both u' and L_{11} are kept unchanged. This implies that $u'/S_{b\left(\phi_g\right)}$ and $L_{11}/\delta_{\left(\phi_g\right)}$values are different for $\phi_{ov}=0.8$ (i.e. $u'/S_{b\left(\phi_g=0.8\right)} = 6.66$ and $L_{11}/\delta_{\left(\phi_g=0.8\right)} = 1.47$) and 1.2 (i.e. $u'/S_{b\left(\phi_g=1.2\right)} = 4.76$ and $L_{11}/\delta_{\left(\phi_g=1.2\right)} = 2.77$) cases where $\delta_{\left(\phi_g\right)}$ is the thermal flame thickness for the equivalence ratio ϕ_g. The simulation parameters used here have been summarised in Table 1. It is worth noting that due to strict resolution requirements of DNS, it becomes extremely computationally demanding to carry out a parametric analysis for experimental conditions, such as reported in Refs. [1, 11], especially for the scale separation between L_{11} and δ_{st} used in experiments. Therefore a direct quantitative comparison with experimental data is not attempted in this analysis. However, the computational findings from this database [35, 37] reveal that the presence of large droplets augments the rate of burning for overall fuel-lean mixtures, whereas an opposite trend is observed for overall fuel-rich and stoichiometric mixtures, and these findings remain in qualitative agreement with previous experimental observations [11]. Furthermore, the droplet-induced wrinkling effects are discernible only for small turbulence intensities, as reported in previous experimental [1, 11] and computational [35, 37] analyses and that is why low turbulence intensities are intentionally chosen for this analysis. For example, the $u'/S_{b\left(\phi_g\right)}$ values chosen by Lawes and Saat [11] are 0, 1.1 and 8.0, and not much difference between gaseous and spray flames was observed for $u'/S_{b\left(\phi_g\right)} = 8.0$. Thus, the turbulence intensity used in this analysis remains comparable to previous experimental investigation by Lawes and Saat [11]. The magnitude of mixture fraction gradient for flame extinction can be estimated as $|\nabla\xi|_{ext} = \xi_{st}(1-\xi_{st})S_{b\left(\phi_g=1\right)}/\sqrt{2}\alpha_{T0}$ [88]. The maximum value of $|\nabla\xi|$ has been found to be smaller than $0.5|\nabla\xi|_{ext}$ based on the laminar spray flame simulations used for initial condition specification and a qualitatively similar conclusion has been obtained for the turbulent spray flames considered here. Therefore, local flame extinction is not expected for the cases considered in this study. The droplet size needs to be much smaller than the computational grid size for the validity of point source assumption and thus, the large droplets and large droplet density which may lead to local flame extinction are not encountered in the cases considered here.

The simulation time considered here (i.e. $t_{sim} = 2.52t^+ = 2.52\alpha_{T0}/S^2_{b\left(\phi_g=1\right)}$) remains comparable to a number of previous DNS analyses [66, 70–75, 89, 90], which provided valuable physical insights into the fundamental understanding of turbulent combustion. The turbulent kinetic energy evaluated over the whole domain does not vary rapidly with time at $t = 2.52\alpha_{T0}/S^2_{b\left(\phi_g=1\right)}$. The rms velocity fluctuation evaluated over the whole domain decayed by about 40% when the statistics were extracted (i.e. $t_{sim} = 2.52t^+ = 2.52\alpha_{T0}/S^2_{b\left(\phi_g=1\right)}$).

The normalised initial droplet number density ρ_N is given by: $1.28 \leq (\rho_N)^{1/3}\delta_{st} \leq 2.19$ in the unburned gas, and the liquid volume fraction remains well below 0.01. The droplet diameter remains smaller than the Kolmogorov length scale for all cases and the ratio of initial droplet diameter to the Kolmogorov length scale is $a_d/\eta = 0.15, 0.19, 0.23$ for $a_d/\delta_{st} = 0.04, 0.05, 0.06$ respectively. The Stokes number, being smaller than 0.18 for the turbulent cases considered here, is given by $St = \tau_u\sqrt{k}/L_{11} = \rho_d a_d^2\sqrt{k}/(18C_u\mu L_{11})$ (where $\tau_u = \rho_d a_d^2/18C_u\mu$ is the particle time scale and $L_{11}/\sqrt{k}$ is the turbulent time scale). An alternative Stokes number $St' = \tau_p S^2_{b(\phi_g=1)}/\alpha_{T0} = \rho_d a_d^2 S^2_{b(\phi_g=1)}/(18C_u\mu\alpha_{T0})$ can be estimated based on the chemical time scale $\alpha_{T0}/S^2_{b(\phi_g=1)}$ and the maximum value of St' remains smaller than 0.3 for the largest droplets considered in this analysis. The mean normalised inter-droplet distance s_d/η varies between 2.47 and 3.71. The ratio of the initial droplet diameter to grid spacing considered in this study remains comparable to several previous analyses [66, 70–75]. Due to the high volatility of n-heptane, the size of droplets decreases significantly (≥50%) by the time they reach the reaction zone. Thus, the droplets, which interact with the flame, are much smaller than the initial size of the droplets. Thus, the assumption of sub-grid evaporation is not expected to affect the statistics of flame-droplet interaction analysed in this paper.

4 Results and Discussion

4.1 Flame-turbulence interaction

Instantaneous distributions of reaction progress variable, c and gaseous equivalence ratio, ϕ_g on the central x-y mid-plane at $t = 2.52\alpha_{T_0}/S^2_{b(\phi_g=1)}$ are shown in Fig. 1 for various overall equivalence ratios $\phi_{ov} = 0.8, 1.0, 1.2$ with initial turbulence intensity of $u'/S_{b(\phi_g=1)} = 4.0$. The droplets residing on the considered plane are illustrated by grey dots. It can be seen from Fig. 1 that the flame-turbulence interaction gives rise to considerable flame wrinkling for all cases but droplets also induce additional flame wrinkling in spray flames. It is apparent from Fig. 1a that the cases with $\phi_{ov} = 0.8$ exhibit comparatively smaller burned gas volume, which is not only valid for this mid-plane but also for the three-dimensional flame kernel in its entirety (see later in the paper). Moreover, the reaction progress variable contours in the $\phi_{ov} = 0.8$ cases show significant amount of local flame thickening in comparison to the other cases. It can be seen from Fig. 1a (see 1st column and 2nd row of Fig. 1a) that the liquid droplets shrink in size due

Table 1 Simulation parameters considered in the analysis

a_d/δ_{st}	ϕ_{ov}	r_0/δ_{st}	τ	$u'/S_{b(\phi_g=1)}$	L_{11}/δ_{st}
0.04, 0.05,0.06	0.8, 1.0, 1.2	2.0	6.54	4.0	2.5
Pr	Le	$\gamma = C_p^g/C_v^g$		St	
0.7	1.0	1.4		<0.18	

to evaporation when they approach the flame. The evaporation rate is high for small droplets with initial $a_d/\delta_{st} = 0.04$ due to their large surface to volume ratios, which leads to almost complete evaporation of these droplets by the time they reach the reaction zone. However larger droplets (e.g. droplets with initial $a_d/\delta_{st} = 0.06$) can survive longer and penetrate through the flame. These droplets continue evaporating and release gaseous fuel vapour in the gaseous phase as they travel through the flame. The evaporation of droplets in the unburned gas is not sufficient to produce $\phi_g \approx \phi_{ov}$ and gives rise to predominantly $\phi_g < 1.0$ mixtures in the unburned gas side but the evaporation within the flame and in the burned gas region creates localised fuel-rich (i.e. $\phi_g > 1.0$) pockets and this tendency is prevalent for large droplets due to their slow evaporation rates. In the burned gas side of the flame, large droplets (i.e. droplets with initial $a_d/\delta_{st} = 0.06$) create locally fuel-rich pockets even for cases with $\phi_{ov} = 0.8$. A part of the evaporated fuel in the burned gas diffuses into the flame and burns within the flame due to the presence of excess oxygen diffusing from the unburned gas side. However, Fig. 1b indicates that combustion in the gaseous phase predominantly takes place in mixtures corresponding to $\phi_g < \phi_{ov}$, and this can be substantiated from the probability density functions (PDFs) of normalised mixture fraction ξ/ξ_{st} within the flame (i.e. $0.01 \leq c \leq 0.99$), which are presented in Fig. 2. It is apparent from Fig. 2 that combustion in droplet cases with $\phi_{ov} = 0.8$ mainly takes place under fuel-lean mode (i.e. $\xi/\xi_{st} < 1.0$). However, it is possible to obtain local pockets of fuel-rich and stoichiometric mixtures in the $\phi_{ov} = 0.8$ case for large droplets (i.e. initial $a_d/\delta_{st} = 0.05$ and 0.06 cases) in spite of predominance of fuel-lean mixtures within the flame. The most probable value of ξ/ξ_{st} remains unity in the $\phi_{ov} = 1.0$ cases but the probability of finding fuel-lean mixtures (i.e. $\xi/\xi_{st} < 1.0$) dominates over that of finding stoichiometric and fuel-rich mixtures (i.e. $\xi/\xi_{st} \geq 1.0$). Large droplets (e.g. initial $a_d/\delta_{st} = 0.05$ and 0.06 cases) for $\phi_{ov} = 1.0$ and 1.2 show relatively higher probabilities of finding fuel-rich mixtures but the likelihood of obtaining mixtures with $\phi_g < \phi_{ov}$ remains greater than that of finding mixtures with $\phi_g \geq \phi_{ov}$. The probability of obtaining fuel-lean mixtures increases with increasing droplet diameter because of slower evaporation rate of larger droplets and due to lower number density, which naturally promotes mixture inhomogeneity.

As the probability of finding fuel-lean (i.e. $\phi_g < 1.0$) mixtures is higher in the $\phi_{ov} = 0.8$ cases than in the $\phi_{ov} = 1.0$ and 1.2 cases (see Fig. 1b), the flame thickness $\delta \sim \alpha_{T0}/S_{b(\phi_g)}$ in the $\phi_{ov} = 0.8$ case is expected to the greater than that in the other ϕ_{ov} values because $S_{b(\phi_g)}$ decreases with decreasing ϕ_g in fuel-lean mixtures. The initial Damköhler number (i.e. $Da_{(\phi_g)} = L_{11}S^2_{b(\phi_g)}/u'\alpha_{T0}$) is 0.47, 1.31 and 0.93 for the premixed flames with $\phi_g = 0.8$, 1.0 and 1.2, respectively for initial $u'/S_{b(\phi_g=1)} = 4.0$. The corresponding Karlovitz number values (i.e. $Ka_{(\phi_g)} = \left(u'/S_{b(\phi_g)}\right)^{1.5}\left(L_{11}S_{b(\phi_g)}/\alpha_{T0}\right)^{-0.5}$) are 9.70, 3.50 and 4.85 for $\phi_g = 0.8$, 1.0 and 1.2, respectively. The values of Damköhler (Karlovitz) number for the droplet cases are likely to be smaller (greater) than the corresponding premixed flame cases as a result of combustion of predominantly leaner fuel-air mixture. These Damköhler and Karlovitz number values are representative of the distributed burning regime, and thus these cases are expected to exhibit local flame thickening. These tendencies are particularly strong for the droplet cases with small (large) values of Da (Ka). For this reason, the effects of local flame thickening are most prominent in the $\phi_{ov} = 0.8$ droplet cases, especially for large droplets.

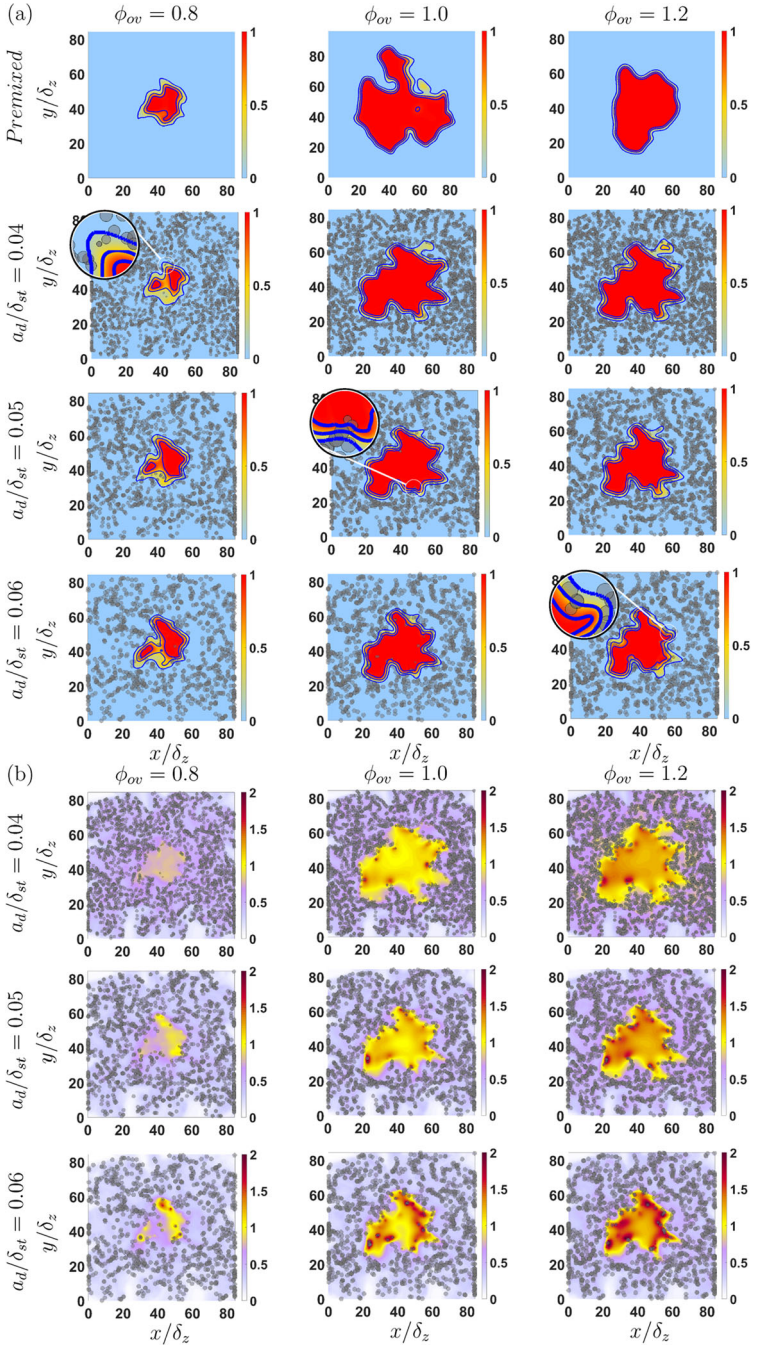

Fig. 1 Distribution of (**a**) reaction progress variable, c (blue lines show $c = 0.1$, 0.5 and 0.9 contours from outer to inner periphery) and (**b**) gaseous equivalence ratio, ϕ_g on the central x-y mid-plane for $\phi_{ov} = 0.8$, 1.0 and 1.2 cases with initial $a_d/\delta_{st} = 0.04$, 0.05 and 0.06. Grey dots show the droplets residing on the plane (not to the scale). All figures and tables correspond to time $t = 2.52\alpha_{T_0}/S^2_{b(\phi_g=1)}$

4.2 Flame-droplet interaction

In order to illustrate the effects of flame-droplet interaction, the instantaneous views of the $c = 0.8$ isosurface (where the maximum value of the reaction rate of reaction progress variable $\dot{w}_c$ is obtained and thus is considered to be the flame surface for the rest of this analysis) are shown in Fig. 3 where the isosurfaces are coloured by the local normalised values of mean curvature $\kappa_m \times \delta_{st} = 0.5(\kappa_1 + \kappa_2) \times \delta_{st}$ and Gauss curvature $\kappa_g \times \delta_{st}^2 = \kappa_1 \kappa_2 \times \delta_{st}^2$ where κ_1 and κ_2 are two principal curvatures [91]. The quantities κ_g and κ_m can be used to identify flame surface topologies. For example, negative (positive) values of κ_m with positive values of κ_g represent cup concave (convex) topologies and negative κ_g values indicate hyperbolic saddle geometries. A zero value of κ_g implies either tile convex (for $\kappa_m > 0$) or tile concave (for $\kappa_m < 0$) or flat surface (for $\kappa_m = 0$) topologies.

It can be seen from Fig. 3a that the premixed gaseous cases exhibit a smooth flame surface with moderate positive and negative values of $\kappa_m \times \delta_{st}$ for all values of equivalence ratio. Spray flames show a qualitatively similar behaviour as that of the premixed gaseous flames for $\phi_{ov} = 0.8$ but dimples can be seen on the flame surface for the spray cases with $\phi_{ov} = 1.0$ and 1.2. These dimples originate due to flame-droplet interaction and similar droplet induced flame wrinkling was reported in experiments by Hayashi *et al.* [1], Lawes and Saat [11] and Thimothée *et al.* [16]. Flame morphology in laminar spherically expanding spray flames was compared with laminar gaseous premixed flames by Thimothée *et al.* [16]. It was observed by Thimothée *et al.* [16] that gaseous premixed flames exhibit a smooth flame surface, whereas the presence of droplets induces deformation of spray flame surfaces. They also demonstrated that the droplet-induced flame wrinkling strengthens with increasing overall equivalence ratios and droplet diameter, which is qualitatively consistent with the present numerical findings. The spray flames for $\phi_{ov} = 1.0$ exhibit dimples with small radii of curvature, which is reflected in their large negative mean curvature values. The dimples on the flame surface of spray flames with $\phi_{ov} = 1.2$ are shallower than the corresponding $\phi_{ov} = 1.0$ cases because of the greater likelihood of more droplets interacting with the flame surface due to larger number density in the $\phi_{ov} = 1.2$ cases.

The most probable value of normalised Gauss curvature $\kappa_g \times \delta_{st}^2$ remains mostly close to zero in the gaseous premixed cases, which indicates the dominance of tile type flame

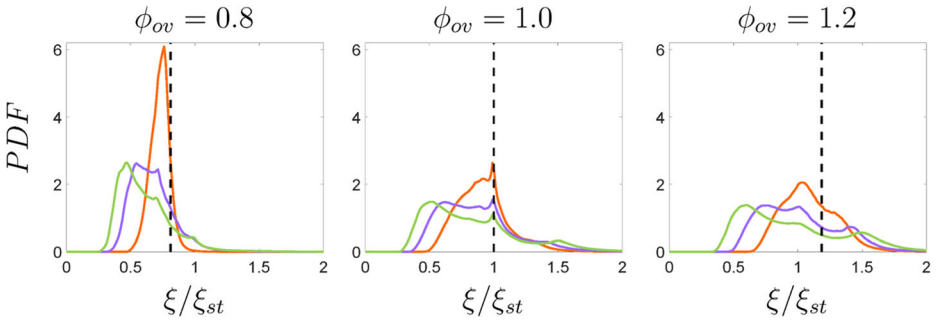

Fig. 2 PDF of mixture fraction normalised by its stoichiometric value ξ/ξ_{st} in the flame (i.e. $0.01 \leq c \leq 0.99$) for droplet cases with initial droplet diameters $a_d/\delta_{st} = 0.04$ (—), 0.05 (—) and 0.06 (—) at $t = 2.52\alpha_{T_0}/S_{b(\phi_g=1)}^2$. The vertical black line indicates the value of ξ/ξ_{st} corresponding to the ϕ_{ov} value of the cases considered here

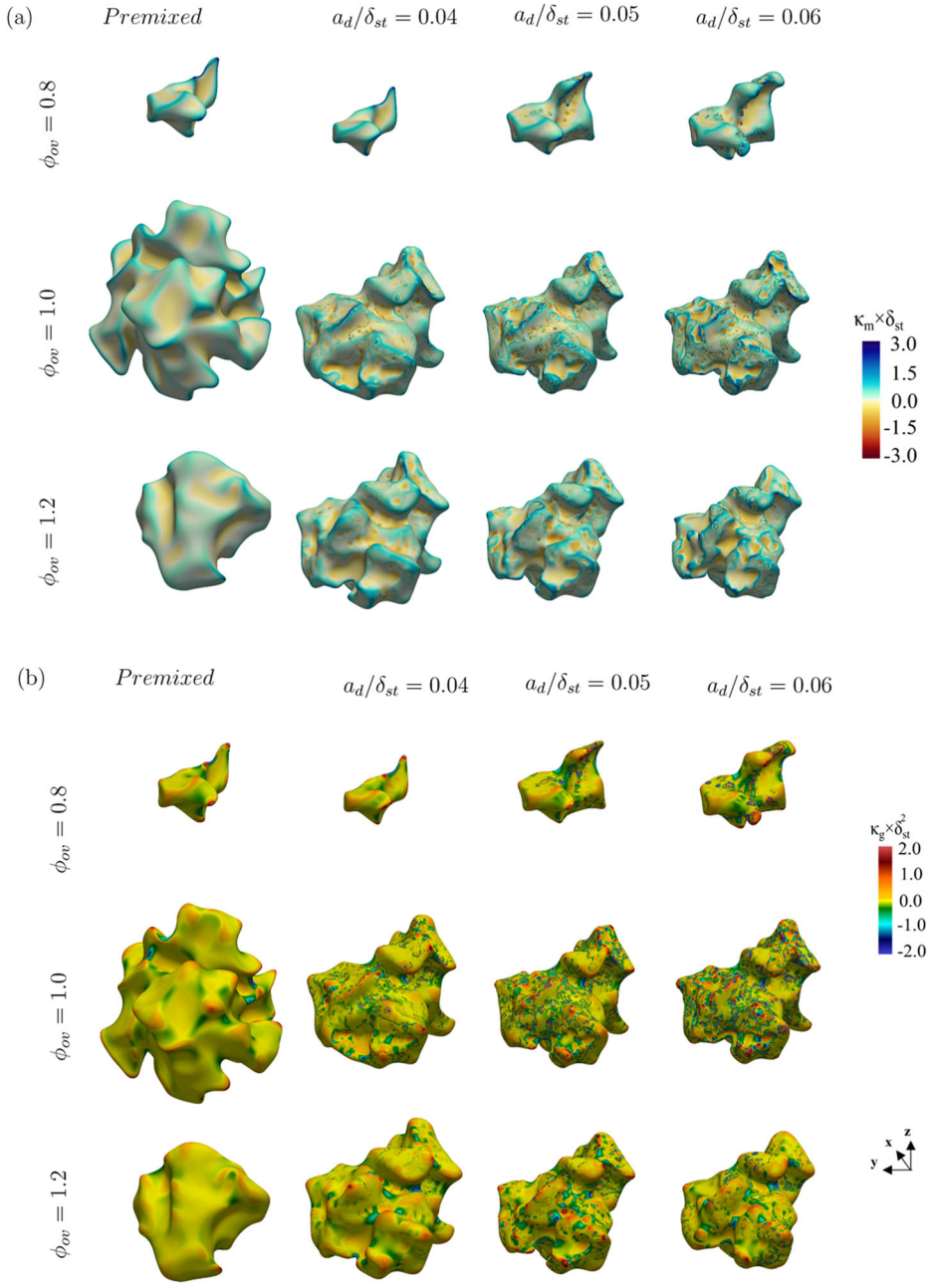

Fig. 3 Instantaneous view of $c = 0.8$ isosurface coloured with normalised **a** mean curvature $\kappa_m \times \delta_{st}$ and **b** Gauss curvature $\kappa_g \times \delta_{st}^2$ for premixed gaseous (1st column) and droplet (2nd-4th columns) cases with initial $\phi_{ov} = 0.8$ (1st and 4th rows), $\phi_{ov} = 1.0$ (2nd and 5th rows) and $\phi_{ov} = 1.2$ (3rd and 6th rows) at $t = 2.52\alpha_{T_0}/S^2_{b(\phi_g=1)}$

topologies. This is found to be consistent with previous findings by Jenkins and Cant [20]. Moreover, the flame surface in the spray cases shows considerable probability of finding

negative $\kappa_g \times \delta_{st}^2$ values, which implies saddle convex or concave topologies depending on the sign of $\kappa_m \times \delta_{st}$.

The effects of flame-droplet interaction on flame wrinkling and flame topologies can be quantified with the help of the joint PDFs between $\kappa_g \times \delta_{st}^2$ and $\kappa_m \times \delta_{st}$, which are presented in Fig. 4. The region given by $\kappa_g > \kappa_m^2$ yields complex principal curvatures, and thus is not physically realisable and the boundary of $\kappa_g = \kappa_m^2$ is shown by the parabola in black in Fig. 4. It can be seen from Fig. 4 that the spread of the $\kappa_g \times \delta_{st}^2$ and $\kappa_m \times \delta_{st}$ values in the joint PDFs for the droplet cases is greater than the corresponding premixed flame cases. This is indicative of the droplet-induced flame wrinkling in the droplet cases, which is consistent with the observations made from Fig. 3. Figure 4 shows that the likelihood of obtaining $\kappa_m > 0$ is greater than that of $\kappa_m < 0$ for all cases considered here because these spherically expanding cases are expected to exhibit flame surface elements, which are predominantly convex to the unburned mixture. It can be seen from Fig. 4 that the cases with $\phi_{ov} = 0.8$ show a higher probability of finding cup convex topologies than the corresponding $\phi_{ov} = 1.0$ and 1.2 cases because of the smaller mean flame radius and burned gas volume due to mostly fuel-lean combustion for $\phi_{ov} = 0.8$ (see Fig. 1a). Moreover, the probability of finding saddle topologies increases with increasing droplet size for all values of overall equivalence ratio due to the increased extent of droplet-induced flame wrinkling. However, the flame surface in large droplet cases (i.e. initial $a_d/\delta_{st} = 0.05$ and 0.06) for $\phi_{ov} = 0.8$ exhibits predominantly convex saddle toplogoies, whereas the flame surfaces in $\phi_{ov} = 1.0$ and 1.2 cases exhibit considerable probability of finding negative saddle topologies due to the significant extent of wrinkling arising from the interaction with the high number density of droplets.

The droplet-induced flame wrinkling acts to increase flame surface area in spherically expanding flames propagating into droplet mists. The variations of normalised burning rate Ω^+ and flame surface area A^+ for different initial droplet diameters and overall equivalence ratios are listed in Table 2. The normalised burning rate Ω^+ and flame surface area A^+ are evaluated as $\Omega^+ = \left(1/\left(\rho_0 S_{b(\phi_g=1)} 4\pi r_0^2\right)\right)\int_V \dot{w}_c dV$ and $A^+ = \left(1/4\pi r_0^2\right)\int_V |\nabla c| dV$, respectively. It can be seen from Table 2 that flame surface area and volume integrated burning rate for the spray flame cases with large droplets (i.e. initial $a_d/\delta_{st} = 0.05$ and 0.06) are found to be greater than the corresponding gaseous premixed flame case for $\phi_{ov} = 0.8$ and this tendency strengthens with increasing a_d/δ_{st}. However, both Ω^+ and A^+ values for the initial $a_d/\delta_{st} = 0.04$ case for $\phi_{ov} = 0.8$ are smaller than the corresponding gaseous premixed flame case. By contrast, both Ω^+ and A^+ increase with decreasing a_d/δ_{st} for $\phi_{ov} = 1.0$ and 1.2 and these values for the spray flame cases are found to be smaller than the corresponding gaseous premixed flame cases. These findings are qualitatively consistent with the experimental results by Hayashi *et al.* [1] and Lawes and Saat [11].

The evaporation rates are high for small droplets, and thus the evaporated gaseous fuel gets more time to mix with the surrounding air before combustion than in the case of larger droplets. Moreover, the extent of droplet-induced flame wrinkling and flame area generation increases with increasing droplet size. For $\phi_{ov} = 0.8$ cases with initial $a_d/\delta_{st} = 0.04$, the droplet-induced flame wrinkling remains weak (see Figs. 3 and 4) and combustion takes place in a gaseous mixture with overwhelming probability of finding $\phi_g < 0.8$ in spite of relatively rapid evaporation of small droplets (see Fig. 2). This gives rise to both smaller burned gas volume and accordingly smaller flame surface area in the case with initial $a_d/\delta_{st} = 0.04$ and the corresponding gaseous premixed flame case for $\phi_{ov} = 0.8$. However, relatively slower

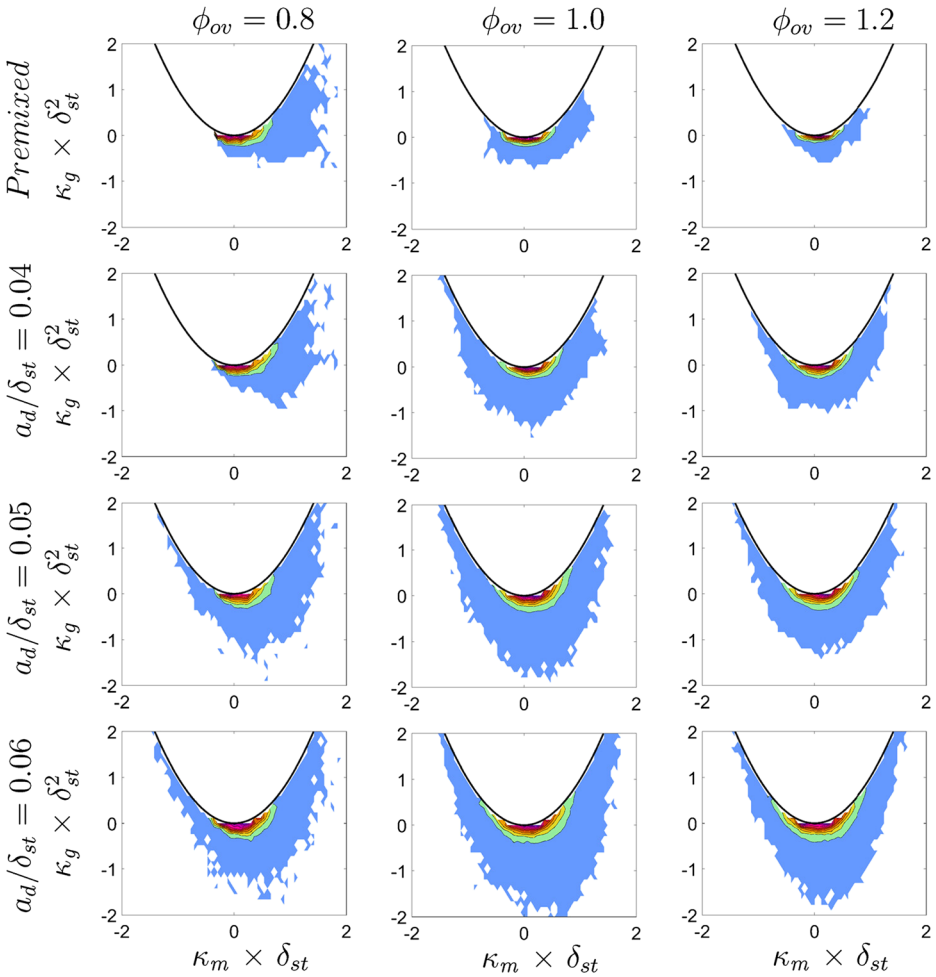

Fig. 4 Joint PDFs of normalised mean curvature $\kappa_m \times \delta_{st}$ and normalised Gauss curvature $\kappa_g \times \delta_{st}^2$ on $c = 0.8$ isosurface for premixed and spray flames with different overall equivalence ratios (1st-3rd column)

evaporation rate in the $\phi_{ov} = 0.8$ cases with initial $a_d/\delta_{st} = 0.05$ and 0.06 in comparison to the initial $a_d/\delta_{st} = 0.04$ case, gives rise to the higher probability of finding more reactive fuel-air mixture than $\phi_g > 0.8$ within the flame (see Fig. 2) and this tendency strengthens with increasing droplet diameter. This along with the increasing extent of droplet-induced flame wrinkling with increasing a_d/δ_{st} gives rise to the increasing trends of Ω^+ and A^+ with increasing

Table 2 Normalised burning rate Ω^+ and normalised flame surface area A^+ values for the cases considered in this study. G P in the table header refers to the gaseous premixed flame case

	$\phi_{ov} = 0.8$				$\phi_{ov} = 1.0$				$\phi_{ov} = 1.2$			
a_d/δ_{st}	0.04	0.05	0.06	G P	0.04	0.05	0.06	G P	0.04	0.05	0.06	G P
Ω^+	2.66	5.97	6.58	3.80	34.15	25.45	23.59	66.02	32.70	23.28	17.47	27.66
A^+	8.03	13.48	15.25	10.45	42.29	35.01	34.97	71.81	42.89	34.42	30.22	30.59

droplet size for $\phi_{ov} = 0.8$. It can be seen from Fig. 1b that gaseous phase combustion takes place predominantly under fuel-lean mode[1] in the $\phi_{ov} = 1.0$ and 1.2 cases (see Fig. 2) and this tendency strengthens with increasing droplet size because of the slow evaporation rate of large droplets. This gives rise to overwhelming probability of combustion of less reactive gaseous fuel-air mixture in the droplet cases in comparison to the corresponding gaseous premixed flame cases for $\phi_{ov} = 1.0$ and 1.2, and this tendency strengthens further with increasing droplet size. This, in turn, gives rise to smaller value of the burned gas volume for droplet cases than the corresponding premixed flame cases and thus Ω^+ shows a decreasing trend with increasing a_d/δ_{st} for $\phi_{ov} = 1.0$ and 1.2 cases. This decrease in burned gas volume with increasing a_d/δ_{st} overcomes the effects of increased droplet-induced flame surface wrinkling for larger droplets and gives rise to a decreasing trend of A^+ with increasing a_d/δ_{st} for $\phi_{ov} = 1.0$ and 1.2 cases.

The effects of a_d/δ_{st} and ϕ_{ov} on Ω^+ and A^+ are the outcomes of the variations of flame propagation characteristics in response to the changes in droplet diameter and overall equivalence ratio, which will be discussed next in this paper.

4.3 Statistical analysis of flame speeds

The statistical behaviour of S_d^* is governed by $\dot{w}_c$, $\dot{S}_{liq,c}$, $\dot{A}_c$ and $\nabla\cdot(\rho D\nabla c)$ which appear on the right side of the transport equation of the reaction progress variable, c (see Eq. 11). The mean values of the terms $\dot{w}_c$, $\dot{S}_{liq,c}$, $\dot{A}_c$ and $\nabla\cdot(\rho D\nabla c)$ conditional on c are shown in Fig. 5. The molecular diffusion term $\nabla\cdot(\rho D\nabla c)$ is the only term whose mean value plays a significant role in the preheat zone (i.e. $c < 0.5$) and the mean value of $\nabla\cdot(\rho D\nabla c)$ remains positive in the preheat zone (i.e. $c < 0.5$) for both gaseous premixed and droplet cases. However, in both gaseous premixed and droplet cases the mean value of $\nabla\cdot(\rho D\nabla c)$ assumes negative values in the reaction zone (i.e. $0.9 \le c \le 0.5$) and also towards the burned gas side of the flame. The mean reaction rate $\dot{w}_c$ assumes deterministically positive values, and its peak value is obtained at around c=0.8 for both gaseous premixed and droplet cases. This justifies the choice of the c=0.8 isosurface as the flame surface in this analysis. The positive mean value of $\dot{w}_c$ and negative mean value of $\nabla\cdot(\rho D\nabla c)$ remain in approximate equilibrium in the reaction zone. The mean values of the terms associated with droplet evaporation $\dot{S}_{liq,c}$ and mixture inhomogeneity $\dot{A}_c$ remain much smaller in magnitude in comparison to the magnitudes of the mean values of $\dot{w}_c$ and $\nabla\cdot(\rho D\nabla c)$ throughout the flame irrespective of the values of a_d/δ_{st} and ϕ_{ov}. The same behaviour in terms of relative magnitudes is obtained when the mean values of $\dot{w}_c$, $\dot{S}_{liq,c}$, $\dot{A}_c$ and $\nabla\cdot(\rho D\nabla c)$ conditional on ξ are considered, which are not presented here for the sake of brevity. The highest magnitude of the mean values of $\dot{w}_c$ and $\nabla\cdot(\rho D\nabla c)$ are obtained for $\xi \approx \xi_{st}$ when their mean values are evaluated conditional on ξ. The mean values of $\dot{w}_c$ conditional on ξ for $\phi_{ov} = 1.0$ are presented in Ref. [35] and thus are not presented here and qualitatively similar behaviour has been observed for $\phi_{ov} = 0.8$ and 1.2.

It can be seen from Fig. 5 that the mean value of $\dot{w}_c$ decreases with increasing a_d for $\phi_{ov} =$ 1.0 and 1.2 cases and in these droplet cases the mean value of $\dot{w}_c$ remains smaller than the corresponding gaseous premixed flame case. By contrast, the cases with large droplets (i.e. initial a_d/δ_{st}=0.05 and 0.06) exhibit higher peak mean values of $\dot{w}_c$ increases with increasing a_d/δ_{st}. However, the peak mean value of $\dot{w}_c$ remains smaller than the corresponding premixed

[1] The maximum value of unstrained laminar burning velocity $S_{b(\phi_g)}$ is obtained for $\phi_g \approx 1.1$ for the present thermo-chemistry.

flame case for initial $a_d/\delta_{st}=0.04$ for $\phi_{ov}=0.8$. The mean behaviour of $\dot{w}_c$ is qualitatively consistent with the behaviour of Ω^+ reported in Table 2. As the peak (negative) magnitude of the molecular diffusion rate $\nabla\cdot(\rho D\nabla c)$ is obtained in the reaction zone where it remains in approximate equilibrium with the mean reaction rate $\dot{w}_c$, the variations of the peak magnitudes of $\nabla\cdot(\rho D\nabla c)$ in response to the changes of a_d/δ_{st} and ϕ_{ov} are qualitatively similar to those obtained for the mean values of $\dot{w}_c$.

The PDFs of displacement speed $S_d^*/S_{b(\phi_g=1)}$ and its components $S_i^*/S_{b(\phi_g=1)}$ where ($i=r$, n, t, $z+s$) on $c=0.8$ isosurface are shown in Fig. 6. A comparison of the PDFs $S_d^*/S_{b(\phi_g=1)}$ between premixed gaseous and droplet cases reveals that premixed gaseous flames with ϕ_{ov}=1.0 and 1.2 exhibit higher probability of obtaining positive $S_d^*/S_{b(\phi_g=1)}$ than in droplet cases. In all cases a finite probability of finding negative $S_d^*/S_{b(\phi_g=1)}$ is observed, which suggests that locally the flame moves opposite to the flame normal direction instead of propagating into unburned gases. The negative values of $S_d^*/S_{b(\phi_g=1)}$ are expected in these flames according to the scaling analysis by Peters [88] because all these cases represent $Ka>1$ combustion. As the Karlovitz number values are expected to be higher in the droplet cases than the corresponding gaseous premixed flame because of predominantly fuel-lean combustion, the probability of finding negative $S_d^*/S_{b(\phi_g=1)}$ has been found to be higher in these droplet cases. Moreover, the mean values of $S_d^*/S_{b(\phi_g=1)}$ of the premixed gaseous flames with ϕ_{ov}=1.0 and 1.2 remain greater than the droplet cases. Furthermore, the probability of finding positive values of $S_d^*/S_{b(\phi_g=1)}$ decreases with increasing a_d/δ_{st}. In the case of ϕ_{ov}=0.8, the PDFs of $S_d^*/S_{b(\phi_g=1)}$ for the gaseous premixed flame and the initial $a_d/\delta_{st}=0.04$ case remain comparable but the PDFs of $S_d^*/S_{b(\phi_g=1)}$ for the initial $a_d/\delta_{st}=0.05$ and 0.06 cases show higher probability of finding positive $S_d^*/S_{b(\phi_g=1)}$ than the corresponding premixed flame case. This suggests that the flame kernel propagates faster for increasing droplet diameter for ϕ_{ov}=0.8 and can exhibit faster propagation rate than the corresponding premixed flame. By contrast, the propagation rate of the droplet cases remains smaller than the corresponding premixed flames for ϕ_{ov}=1.0 and 1.2, and the propagation rate decreases with increasing diameter. These findings are consistent with the trends of Ω^+ reported in Table 2.

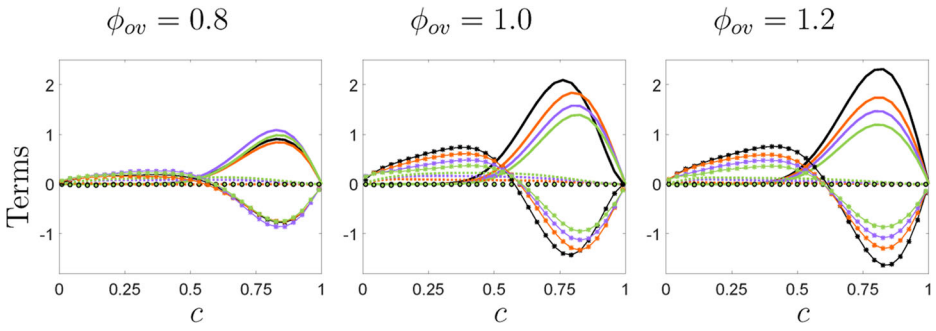

Fig. 5 Variations of mean values of $\dot{w}_c$ (continuous line),$\nabla\cdot(\rho D\nabla c)$ (continuous line with star marker), $\dot{A}_c$ (dotted line) and $\dot{S}_{liq,c}$ (circle marker with black edges) conditional on c for droplet cases with initial $a_d/\delta_{st}=0.04$ (orange color), 0.05 (purple color) and 0.06 (green color) and also for the gaseous premixed case (black color). All terms are normalised by $\delta_{st}/\rho_0 S_{b(\phi_g=1)}$

It is necessary to analyse the statistical behaviours of the different components of $S_d^*/S_{b(\phi_g=1)}$ (see Eq. 13) in order to explain the origin of its negative value, and to isolate different physical mechanisms, which lead to the differences in flame propagation between gaseous premixed and droplet flame cases. The PDFs of $S_r^*/S_{b(\phi_g=1)}$ and $S_n^*/S_{b(\phi_g=1)}$ exhibit positive and negative values, respectively in the reaction zone, and they exhibit wider distributions for droplet cases than the corresponding premixed flame cases. The variations of equivalence ratio give rise to a large spread of values of $\dot{w}_c$ and $|\nabla c|$ on a given c isosurface, which contribute to the larger spreads of the values of $S_r^*/S_{b(\phi_g=1)}$ and $S_n^*/S_{b(\phi_g=1)}$ in the droplet cases than in the corresponding premixed cases. The PDFs of normalised tangential diffusion component of displacement speed $S_t^*/S_{b(\phi_g=1)} = -2\rho D\kappa_m/\rho_0 S_{b(\phi_g=1)}$ exhibit predominantly negative values for all cases due to the predominance of positive κ_m (i.e. convex flame topologies), as shown in Fig. 4. The PDFs of $S_t^*/S_{b(\phi_g=1)}$ for the droplet cases are wider than the corresponding premixed flames because of wider curvature distributions (see Fig. 4) arising from droplet-induced flame wrinkling. The positive $S_r^*/S_{b(\phi_g=1)}$, and negative $S_n^*/S_{b(\phi_g=1)}$ and $S_t^*/S_{b(\phi_g=1)}$ values at $c = 0.8$ are consistent with the mean variations of $\dot{w}_c$ and $\nabla\cdot(\rho D\nabla c)$ shown in Fig. 5.

It can be seen from Fig. 6 that the probability of finding high positive (negative) values of $S_r^*/S_{b(\phi_g=1)}$ ($S_n^*/S_{b(\phi_g=1)}$) decreases with increasing a_d for $\phi_{ov} = 1.0$ and 1.2 cases and in these droplet cases the mean and most probable values of $S_r^*/S_{b(\phi_g=1)}$ and the magnitude of the mean and the most probable $S_n^*/S_{b(\phi_g=1)}$ remain smaller than the corresponding gaseous premixed flame case. By contrast, the cases with large droplets (e.g. initial $a_d/\delta_{st} = 0.05$ and 0.06 cases) exhibit higher probability of finding positive (negative) values of $S_r^*/S_{b(\phi_g=1)}$ ($S_n^*/S_{b(\phi_g=1)}$) than the corresponding premixed flame case for $\phi_{ov} = 0.8$ and the most probable value of $S_r^*/S_{b(\phi_g=1)}$ and the magnitude of the most probable negative value of $S_n^*/S_{b(\phi_g=1)}$ increases with increasing a_d/δ_{st}.

The PDFs of the normalised values of the components associated with droplet evaporation and mixture inhomogeneity $S_{z+s}^*/S_{b(\phi_g=1)}$ are presented together in Fig. 6. It can be seen from Fig. 6 that the PDFs of $S_{z+s}^*/S_{b(\phi_g=1)}$ peak around zero (i.e. the most probable value remains close to zero) for all droplet cases but a long positive tail is observed for positive values for large droplets (i.e. initial $a_d/\delta_{st} = 0.05$ and 0.06 cases). This is also consistent with the observations made from Fig. 5, which revealed that the magnitudes of the mean values of the terms associated with droplet evaporation $\dot{S}_{liq,c}$ and mixture inhomogeneity $\dot{A}_c$ remain much smaller than the magnitudes of the mean values of $\dot{w}_c$ and $\nabla\cdot(\rho D\nabla c)$ for all values of a_d/δ_{st} and ϕ_{ov}. This is also found to be consistent with the previous findings by Wacks *et al.* [69] in the case of statistically planar flames propagating into droplet-laden mixtures.

It can be inferred from Fig. 6 that locally negative values of $S_d^*/S_{b(\phi_g=1)}$ are obtained when the negative values of $S_{n+t}^*/S_{b(\phi_g=1)}$ overcome the positive contribution of $S_r^*/S_{b(\phi_g=1)}$.

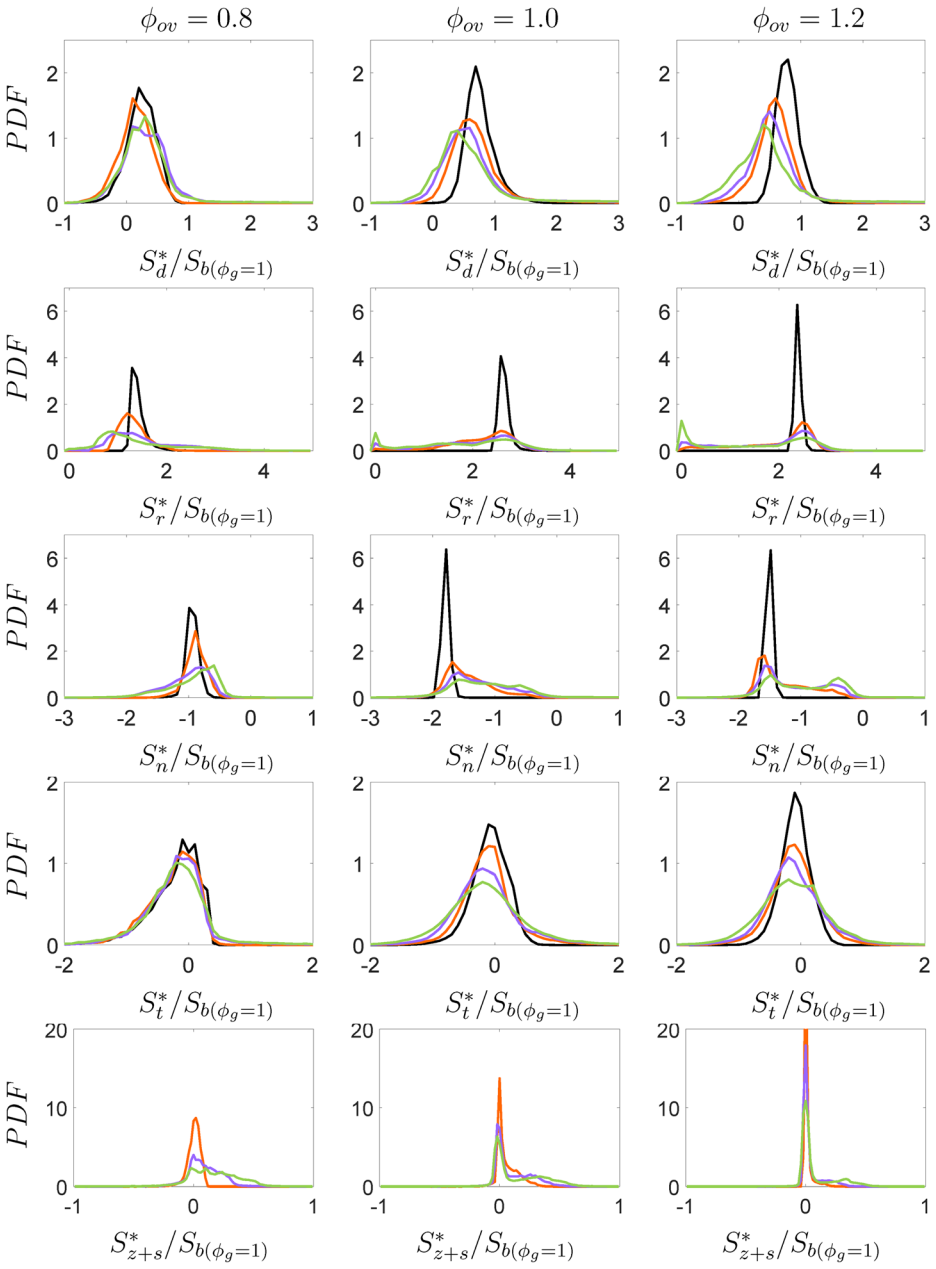

Fig. 6 PDFs of $S_i^*/S_{b(\phi_g=1)}$ (1st-5th rows) where ($i = d, r, n, t, z+s$) on $c = 0.8$ for droplet cases with initial $a_d/\delta^{st} = 0.04$ (—), 0.05 (—) and 0.06 (—) and for premixed gaseous case (—)

However, in all cases the probability of finding positive values of $S_d^*/S_{b(\phi_g=1)}$ supersedes that of finding negative values, which suggests that the flame kernels grow in size with time for all cases considered here in spite of local instances where the flame retreats into the burned gas instead of propagating into the unburned gas.

The PDFs of normalised consumption and displacement speeds (i.e. $S_c/S_{b(\phi_g=1)}$ and $S_d^*/S_{b(\phi_g=1)}$) are compared in Fig. 7 for all cases considered here. It can be seen from Fig. 7 that the consumption speed remains deterministically positive, whereas the PDF of $S_d^*/S_{b(\phi_g=1)}$ exhibits finite probability of finding negative values although the mean value remains positive for all cases (see Fig. 6). As the consumption speed S_c is principally determined by $\dot{w}_c$ (see Eq. 18), the variations of $S_c/S_{b(\phi_g=1)}$ in response to the changes of a_d/δ_{st} and ϕ_{ov} are qualitatively similar to those obtained for $S_r^*/S_{b(\phi_g=1)}$ (see Fig. 6). However, it can be seen from Fig. 7 that the probability of finding positive values of $S_c/S_{b(\phi_g=1)}$ is greater than that in the case of $S_d^*/S_{b(\phi_g=1)}$ for all cases considered here. Furthermore, the most probable value of $S_c/S_{b(\phi_g=1)}$ remains greater than $S_d^*/S_{b(\phi_g=1)}$ for all cases. Moreover, the most probable values of $S_d^*/S_{b(\phi_g=1)}$ remain smaller than $S_{b(\phi_g=\phi_{ov})}/S_{b(\phi_g=1)}$, whereas the most probable values of $S_c/S_{b(\phi_g=1)}$ are found to be comparable to $S_{b(\phi_g=\phi_{ov})}/S_{b(\phi_g=1)}$ for all cases considered here. In the case of unity Lewis number spherically expanding premixed flames, the net positive stretch rate acts to decrease $S_d^*/S_{b(\phi_g=1)}$ in comparison to $S_{b(\phi_g=\phi_{ov})}/S_{b(\phi_g=1)}$ but $S_c/S_{b(\phi_g=1)}$ remains unaffected [92]. The stretch rate effects on $S_d^*/S_{b(\phi_g=1)}$ are further augmented by the higher value of Ka due to the presence of predominantly fuel-lean mixtures in the reaction zone for the droplet cases considered here. Figure 7 further reveals that there is considerable difference between the statistical behaviours and magnitudes of S_c and S_d^*, which is consistent with previous findings [38, 40] in the case of statistically planar premixed turbulent flames. This can be substantiated from the contours of joint PDFs of $S_c/S_{b(\phi_g=1)}$ with $S_d^*/S_{b(\phi_g=1)}$ on $c=0.8$ shown in Fig. 8. It can be seen from Fig. 8 that $S_c/S_{b(\phi_g=1)}$ and $S_d^*/S_{b(\phi_g=1)}$ are weakly negatively correlated for the ϕ_g=0.8 gaseous premixed case, whereas this correlation remains weak with no clear trend for premixed cases with $\phi_g=1.0$ and 1.2. The correlation between $S_c/S_{b(\phi_g=1)}$ and $S_d^*/S_{b(\phi_g=1)}$ remains weakly positive for all droplet cases.

It is worthwhile to note that the consumption speed has been found to be weakly correlated with curvature κ_m and tangential strain rate $a_T=(\delta_{ij}-N_iN_j)\partial u_i/\partial x_j$ for all premixed flame cases considered here and this can be substantiated from the correlation coefficients listed in Table 3. By contrast, S_d^* is negatively correlated with κ_m, whereas a positive correlation is obtained between S_d^* and a_T for the premixed flame cases, as demonstrated by the correlation coefficients listed in Table 3. The physical explanations behind these correlations have been provided elsewhere [25–27] and thus are not repeated here. Moreover, it has been demonstrated in Refs. [26, 27] that the strength of the displacement speed correlations with tangential strain rate and curvature depend on the mean flame radius. Furthermore, the effects of heat release and turbulence evolution within the flame are different for different equivalence ratios, which along with the difference in mean flame radius give rise to differences in correlation strengths of S_d^* with κ_m and a_T between $\phi_g=0.8$, 1.0 and 1.2 premixed turbulent cases. For the droplet cases, a_T and κ_m dependences of S_d^* remain qualitatively similar to the corresponding premixed flames. However, in the droplet cases, the variation of ϕ_g on a given c isosurface gives rise to several qualitatively similar correlation branches with differing strengths. As a result, the net correlations of S_d^* with κ_m and a_T in droplet cases are weaker than the corresponding premixed flame cases, and these correlations weaken with increasing droplet

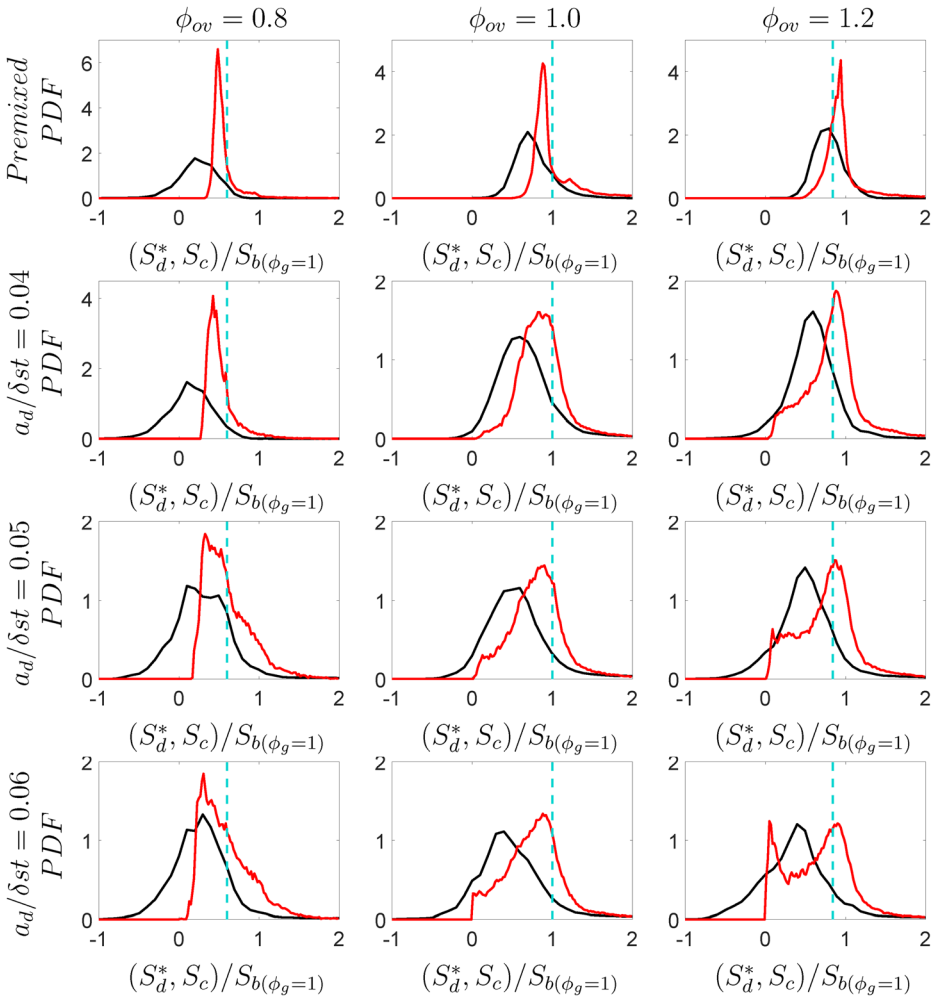

Fig. 7 PDFs of $S_d^*/S_{b(\phi_g=1)}$ (▬) and $S_c/S_{b(\phi_g=1)}$ (▬) on $c = 0.8$ for premixed gaseous case (1st row) and for droplet cases with initial $a^d/\delta^{st} = 0.04$ (2nd row), 0.05 (3rd row) and 0.06 (4th row). The value of $S_{b(\phi_g=\phi_{ov})}/S_{b(\phi_g=1)}$ is shown by the vertical cyan line

diameter as this increases the extent of ϕ_g variations on a given c isosurface (shown in Fig. 2). The combination of weak κ_m and a_T dependences of S_c and relatively stronger curvature and strain rate correlations with S_d^* gives rise to weak interrelation between S_c and S_d^* for all cases. These correlations should not be associated with any physical mechanism because of the small magnitudes of the correlation coefficients irrespective of their signs.

An alternative flame speed can be defined using flame surface area calculations as: $S_A = dr_A/dt$ where the equivalent radius r_A is defined based on flame surface area as: $r_A = \sqrt{A/4\pi}$ and the flame surface area is evaluated using the volume-integral as: $A = \int_V |\nabla c|\, dV$. The value of S_A is calculated by taking the slope of the linear part of the temporal evolution of r_A and this slope remains unchanged since halfway through the simulation for all cases considered here. The flame speed S_A provides a measure of growth rate of flame surface area. Using a similar

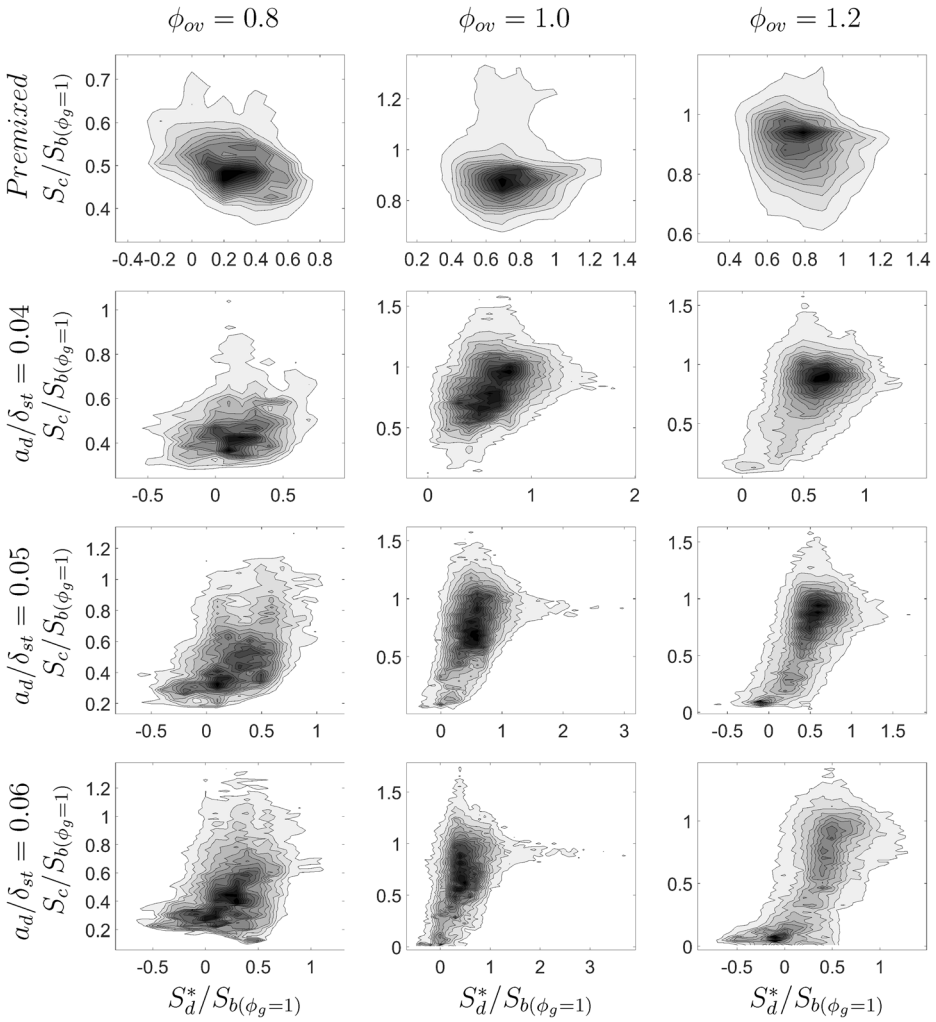

Fig. 8 Contours of joint PDF of $S_c/S_{b\left(\phi_g=1\right)}$ and $S_d^*/S_{b\left(\phi_g=1\right)}$ on $c = 0.8$ isosurface for premixed gaseous cases (1st row) and droplet cases with initial droplet diameters $a^d/\delta^{st} = 0.04$ (2nd row), 0.05 (3rd row) and 0.06 (4th row)

approach another flame speed S_V can be defined as: $S_V = dr_V/dt$ where $r_V = (3V_b/4\pi)^{1/3}$ is an equivalent radius with V_b being the burned gas volume where $c \geq 0.99$ is obtained. Figure 9 shows the variations of $S_A^*/S_{b\left(\phi_g=1\right)} = \rho_b S_A/\left(\rho_0 S_{b\left(\phi_g=1\right)}\right)$ and $S_V^*/S_{b\left(\phi_g=1\right)} = \rho_b S_V/\left(\rho_0 S_{b\left(\phi_g=1\right)}\right)$ along with the mean values of normalised consumption speed $S_c/S_{b\left(\phi_g=1\right)}$ and density-weighted displacement speed $S_d^*/S_{b\left(\phi_g=1\right)}$ on the $c = 0.8$ isosurface for different values of normalised initial droplet diameter a_d/δ_{st} and the overall equivalence ratio ϕ_{ov}, where $\rho_b = m_b/V_b$ is the burned gas density with m_b being the burned gas mass with $c \geq 0.99$. It is evident from Fig. 9 that the mean value of $S_c/S_{b\left(\phi_g=1\right)}$ remains greater than $S_d^*/S_{b\left(\phi_g=1\right)}$ for all values of ϕ_{ov} and a_d/δ_{st}, which is consistent with the findings from Fig. 8.

Table 3 Correlation coefficients for $S_d^*-S_c$, $S_c-\kappa_m$, S_c-a_T, $S_d^*-\kappa_m$ and $S_d^*-a_T$ on the $c=0.8$ isosurface for all cases considered here. G P in the table header refers to the gaseous premixed flame case

		$S_d^*-S_c$	$S_c-\kappa_m$	S_c-a_T	$S_d^*-\kappa_m$	$S_d^*-a_T$
$\phi_{ov}=0.8$	GP	−0.230	0.258	−0.140	−0.870	0.508
	a_d/δ_{st}=0.04	0.109	0.116	0.020	−0.830	0.508
	a_d/δ_{st}=0.05	0.382	0.091	0.162	−0.597	0.378
	a_d/δ_{st}=0.06	0.330	0.132	0.090	−0.457	0.304
$\phi_{ov}=1.0$	GP	0.070	0.004	−0.053	−0.849	0.614
	a_d/δ_{st}=0.04	0.209	0.254	−0.015	−0.592	0.321
	a_d/δ_{st}=0.05	0.258	0.285	0.118	−0.473	0.302
	a_d/δ_{st}=0.06	0.281	0.298	0.129	−0.342	0.263
$\phi_{ov}=1.2$	GP	−0.069	0.098	−0.077	−0.912	0.650
	a_d/δ_{st}=0.04	0.302	0.438	−0.036	−0.344	0.448
	a_d/δ_{st}=0.05	0.337	0.413	0.118	−0.319	0.389
	a_d/δ_{st}=0.06	0.362	0.412	0.215	−0.255	0.357

The presence of droplets enhances the normalised flame speed $S_A^*/S_{b(\phi_g=1)}$ for $\phi_{ov}=0.8$ except for the initial $a_d/\delta_{st}=0.04$ case under turbulent conditions. Normalised flame speed $S_A^*/S_{b(\phi_g=1)}$ increases with increasing droplet diameter for $\phi_{ov}=0.8$, whereas it shows just the opposite behaviour for $\phi_{ov}=1.0$ and 1.2. For $\phi_{ov}=0.8$, large droplets with initial $a_d/\delta_{st}=0.05$ and 0.06 show greater $S_V^*/S_{b(\phi_{g=1})}$ values than that in the case with initial $a_d/\delta_{st}=0.04$. Moreover, $S_V^*/S_{b(\phi_{g=1})}$ in the case of initial $a_d/\delta_{st}=0.05$ for $\phi_{ov}=0.8$ has been found to be greater than that in the corresponding premixed flame case. Furthermore, turbulence significantly affects the normalised flame speed $S_V^*/S_{b(\phi_g=1)}$ and increases the growth rate of burned gas volume for large droplets with $\phi_{ov}=0.8$ and for small droplets with $\phi_{ov}=1.0$ and 1.2. The enhancement of the extent of burning with increasing (decreasing) droplet size for overall fuel-lean (fuel-rich) mixtures is qualitatively consistent with previous experimental findings [11]. The physical explanations for the aforementioned variations of $S_A^*/S_{b(\phi_{g=1})}$ and $S_V^*/S_{b(\phi_{g=1})}$ with a_d/δ_{st} and ϕ_{ov} have been provided elsewhere [35, 37] and thus are not repeated here.

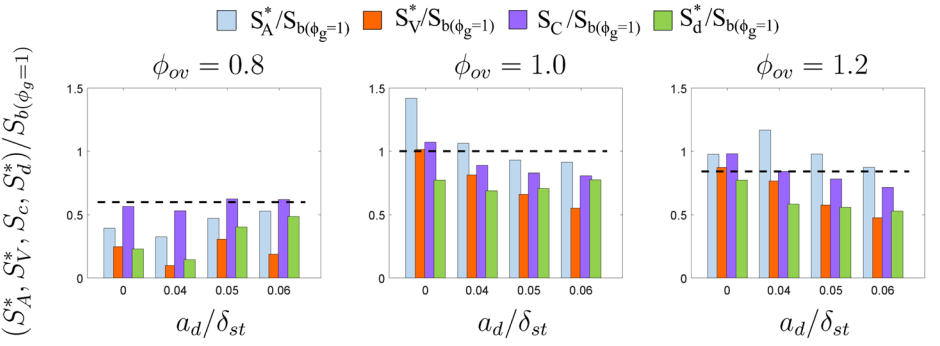

Fig. 9 Mean values of $S_c/S_{b(\phi_g=1)}$ and $S_d^*/S_{b(\phi_g=1)}$ on $c=0.8$ isosurface along with alternative flame speeds $S_A^*/S_{b(\phi_g=1)}$ and $S_V^*/S_{b(\phi_g=1)}$ for the cases with $\phi^{ov}=0.8$, 1.0 and 1.2. The value of $S_{b(\phi_g=\phi_{ov})}/S_{b(\phi_g=1)}$ is shown by the horizontal black dashed line

The horizontal dashed black line in Fig. 9 provides the value of $S_{b\left(\phi_g=\phi_{ov}\right)}/S_{b\left(\phi_g=1\right)}$, which reveals that S_A^* and S_V^* remain smaller than $S_{b\left(\phi_g=0.8\right)}$ in all cases with $\phi_{ov}=0.8$, whereas in the $\phi_{ov}=1.2$ cases S_A^* assumes greater values than $S_{b\left(\phi_g=1.2\right)}$ but S_V^* remains smaller than $S_{b\left(\phi_g=1.2\right)}$. However premixed gaseous case and small droplets with $\phi_{ov}=1.0$ exhibit higher S_A^* values than $S_{b\left(\phi_g=1\right)}$. In premixed gaseous cases with $\phi_{ov}=$ 1.0 and 1.2, S_V^* remains comparable with $S_{b\left(\phi_g=\phi_{ov}\right)}$. The mean values of S_d^* and S_c tend to be smaller than $S_{b\left(\phi_{ov}=\phi_g\right)}$ for all droplet cases irrespective of the values of ϕ_{ov} and a_d, which is consistent with the observations made from Fig. 7. However, the extent of deviation of S_d^* from $S_{b\left(\phi_{ov}=\phi_g\right)}$ is greater than the difference between $S_{b\left(\phi_{ov}=\phi_g\right)}$ and S_c, which is also consistent with theoretical expectations for positively stretched flames [92].

It can be seen from Fig. 9 that the magnitudes of $S_A^*/S_{b\left(\phi_g=1\right)}$ and the mean value of $S_c/S_{b\left(\phi_g=1\right)}$ remain comparable for all cases considered here irrespective of the values of a_d/δ_{st} and ϕ_{ov}. Moreover, the magnitudes of $S_V^*/S_{b\left(\phi_g=1\right)}$ and the mean value of $S_d^*/S_{b\left(\phi_g=1\right)}$ assume comparable values for all cases considered here except for the large droplets (e.g. initial $a_d/\delta_{st}=0.06$) for $\phi_{ov}=0.8$, and the agreement between the mean values of $S_d^*/S_{b\left(\phi_g=1\right)}$ and $S_V^*/S_{b\left(\phi_g=1\right)}$ improves with increasing droplet size for $\phi_{ov}=1.0$ and 1.2. Thus, the findings of Fig. 9 suggest that the evaluation of S_A^* may provide an approximate quantitative estimation of the mean value of S_c but approximating the mean density-weighted displacement speed is a more challenging task. However, the mean density-weighted displacement speed can be approximately estimated by S_V^* for large droplets in the case of overall stoichiometric and fuel-rich mixtures.

5 Conclusions

Three–dimensional carrier phase DNS simulations with modified single-step chemistry have been carried out for turbulent spherically expanding flames propagating into mono-sized n-heptane droplet mists for a range of initial droplet diameters (i.e. $a_d/\delta_{st}=0.04$,0.05 and 0.06) and overall equivalence ratios (i.e. $\phi_{ov}=0.8$, 1.0 and 1.2). The simulation data has been utilised to analyse the flame surface topology and the statistical behaviours of different flame speeds under turbulent conditions for different droplet diameters and overall equivalence ratios. In order to understand the influence of flame-droplet interaction, the combustion characteristics in the droplet cases have been compared with those in corresponding premixed gaseous flames. It has been found that droplets significantly affect the flame surface topology. The presence of droplets leads to dimples on the flame surface for large droplet diameters and large droplet number densities (i.e. overall equivalence ratio), which is reflected in the increased probability of finding high curvature magnitude and wider PDFs of curvature for the droplet cases in comparison to the corresponding gaseous premixed cases. This tendency strengthens with increasing droplet diameter and overall equivalence ratio. However, turbulent gaseous premixed flames exhibit a smooth wrinkled flame surface and this behaviour may prevail for droplet cases with overall fuel-lean equivalence ratios due to the small number of droplets interacting with the flame. Besides dimples on the flame surface, the spray flames show

increased probability of finding saddle topologies in comparison to the corresponding premixed gaseous flames. It has been found that gaseous phase combustion takes place predominantly in fuel-lean mode for all droplet cases considered here including the overall fuel-rich case. The predominance of fuel-lean mixture within the reaction zone for ϕ_{ov}=1.0 and 1.2 cases strengthens further with increasing droplet diameter due to slow evaporation rate. By contrast, the slow evaporation for large droplets gives rise to local islands of fuel-rich and stoichiometric mixtures for the overall fuel-lean $\phi_{ov}=0.8$ case. The mixture composition within the flame and droplet-induced flame wrinkling significantly affect the statistical behaviours of both displacement and consumption speeds. It has been found that the contribution of droplets on the density-weighted displacement speed statistics comes principally through the reaction rate of the mixture arising from mixing of evaporated fuel vapour with surrounding air, and the curvature distribution induced by flame-droplet interaction. The contributions of cross-scalar dissipation arising from mixture inhomogeneity and droplet evaporation remain weak in comparison to the reaction rate and molecular diffusion rate components of the density-weighted displacement speed. It has been found that the probability of finding negative displacement speed increases with increasing droplet diameter for $\phi_{ov}=1.0$ and 1.2, whereas the consumption speed remains deterministically positive due to its sole dependence on reaction rate of reaction progress variable. It has been found that the consumption speed decreases with increasing droplet diameter for $\phi_{ov}=1.0$ and 1.2 and its mean value remains smaller than the corresponding premixed gaseous flames. However, the mean consumption speed has been found to be greater for large droplet cases with $\phi_{ov}=0.8$ than in the corresponding premixed gaseous flames. The mean value of consumption speed remains greater than the mean density-weighted displacement speed for all cases considered here. In addition to consumption and displacement speeds, two additional flame speeds have been considered, which are taken to represent the growth rates of flame surface area and burned gas volume, respectively. These flame speeds have been compared to the mean values of consumption speed and density-weighted displacement speed. The flame speed, which represents the growth rate of flame area, provides an approximate measure of the mean value of the consumption speed, whereas the flame speed representing the growth rate of burned gas volume provides an approximate measure of the mean density-weighted displacement speed for large droplet diameters for $\phi_{ov}=1.0$ and 1.2. Previous simple chemistry DNS analyses [24–27, 46, 47, 50, 52] have been found to capture the flame propagation statistics extracted from detailed chemistry DNS data [43–45, 48, 49, 51] for turbulent premixed flames, and this holds true in particular for curvature effects. Nevertheless, the present findings based on moderate turbulence intensity and simple chemical mechanism need to be validated further for higher values of turbulent Reynolds number (and consequently different Da/Ka) in the presence of detailed chemistry and transport.

Funding The financial support of the Republic of Turkey Ministry of National Education and EPSRC (EP/K025163/1, EP/R029369/1) and the computational support of Rocket and ARCHER are gratefully acknowledged.

Compliance with Ethical Standards

This work did not involve any active collection of human data.

Competing Interests We have no competing interests.

References

1. Hayashi, S., Kumarevgai, S., Sakai, T.: Propagation velocity and structure of flames in droplet-vapor-air mixtures. Combust. Sci. Technol. **15**, 169–177 (1977)
2. Abdel-Gayed, R.G., Al-Khishali, K.J., Bradley, D.: Turbulent burning velocities and flame straining in explosions. Proc. R. Soc. Lond. A. **391**(1801), 393–414 (1984)
3. Beretta, G.P., Rashidi, M., Keck, J.C.: Turbulent flame propagation and combustion in spark ignition engines. Combust. Flame. **52**, 217–245 (1983)
4. Bradley, D., Gaskell, P.H., Gu, X.J.: Burning velocities, Markstein lengths,and flame quenching for spherical methane-air flames, A computational study. Combust. Flame. **104**, 176–198 (1996)
5. Renou, B., Boukhalfa, A., Puechberty, D., Trinité, M.: Local scalar flame properties of freely propagating premixed turbulent flames at various Lewis numbers. Combust. Flame. **123**, 507–521 (2000)
6. Nwagwe, I.K., Weller, H.G., Tabor, G.R., Gosman, A.D., Lawes, M., Sheppard, C.G.W., Wooley, R.: Measurements and large eddy simulations of turbulent premixed flame kernel growth. Proc. Combust. Inst. **28**, 59–65 (2000)
7. Haq, M.Z., Sheppard, C.G.W., Woolley, R., Greenhalgh, D.A., Lockett, R.D.: Wrinkling and curvature of laminar and turbulent premixed flames. Combust. Flame. **131**, 1–15 (2002)
8. Bradley, D., Haq, M.Z., Hicks, R.A., Kitagawa, T., Lawes, M., Sheppard, C.G.W., Woolley, R.: Turbulent burning velocity, burned gas distribution, and associated flame surface definition. Combust. Flame. **133**, 415–430 (2003)
9. Gashi, S., Hult, J., Jenkins, K.W., Chakraborty, N., Cant, R.S., Kaminski, C.F.: Curvature and wrinkling of premixed flame kernels—comparisons of OH PLIF and DNS data. Proc. Combust. Inst. **30**, 809–817 (2005)
10. Hult, J., Gashi, S., Chakraborty, N., Klein, M., Jenkins, K.W., Cant, R.S., Kaminski, C.F.: Measurement of flame surface density for turbulent premixed flames using PLIF and DNS. Proc. Combust. Inst. **31**(I), 1319–1326 (2007)
11. Lawes, M., Saat, A.: Burning rates of turbulent iso-octane aerosol mixtures in spherical flame explosions. Proc. Combust. Inst. **33**, 2047–2054 (2011)
12. Lawes, M., Ormsby, M.P., Sheppard, C.G.W., Woolley, R.: The turbulent burning velocity of iso-octane/air mixtures. Combust. Flame. **159**, 1949–1959 (2012)
13. Chaudhuri, S., Wu, F., Zhu, D., Law, C.K.: Flame speed and self-similar propagation of expanding turbulent premixed flames. Phys. Rev. Lett. **108**(4), 044503–0441–5 (2012)
14. Akkerman, V., Chaudhuri, S., Law, C.K.: Accelerative propagation and explosion triggering by expanding turbulent premixed flames. Phys. Rev. E. **87**(23008), (2013)
15. Brequigny, P., Endouard, C., Mounaïm-Rousselle, C., Foucher, F.: An experimental study on turbulent premixed expanding flames using simultaneously Schlieren and tomography techniques. Exp. Therm. Sci. **95**, 11–17 (2018)
16. Thimothée, R., Chauveau, C., Halter, F. and Gökalp I., Characterization of cellular instabilities of a flame propagating in an aerosol, Proc. of ASME Turbo Expo 2015, GT2015–44022, Canada, (2015)
17. Baum, M., Poinsot, T.: Effects of mean flow on premixed flame ignition. Combust. Sci. Technol. **106**, 19–39 (1995)
18. Poinsot, T., Candel, S., Trouve, A.: Applications of direct numerical simulation to premixed turbulent combustion. Prog. Energy Combust. Sci. **21**, 531–576 (1995)
19. Schmid, H.-P., Habisreuther, P., Leuckel, W.: A model for calculating heat release in premixed turbulent flames. Combust. Flame. **113**, 79–91 (1998)
20. Jenkins, K.W., Cant, R.S.: Curvature effects on flame kernels in a turbulent environment. Proc. Combust. Inst. **29**, 2023–2029 (2002)
21. Tabor, G., Weller, H.G.: Large eddy simulation of premixed turbulent combustion using flame surface wrinkling model. Flow Turbul. Combust. **72**, 1–27 (2004)
22. van Oijen, J.A., Groot, G.R.A., Bastiaans, R.J.M., de Goey, L.P.H.: A flamelet analysis of the burning velocity of premixed turbulent expanding flames. Proc. Combust. Inst. **30**, 657–664 (2005)
23. Thevenin, D.: Three-dimensional direct simulations and structure of expanding turbulent methane flames. Proc. Combust. Inst. **30**, 629–637 (2005)
24. Klein, M., Chakraborty, N., Jenkins, K.W., Cant, R.S.: Effects of initial radius on the propagation of premixed flame kernels in a turbulent environment. Phys. Fluids. **18**(5), 055102 (2006)
25. Jenkins, K.W., Klein, M., Chakraborty, N., Cant, R.S.: Effects of strain rate and curvature on the propagation of a spherical flame kernel in the thin-reactionzones regime. Combust. Flame. **145**, 415–434 (2006)
26. Klein, M., Chakraborty, N., Cant, R.S.: Effects of turbulence on self-sustained combustion in premixed flame kernels, a direct numerical simulation (DNS) study. Flow Turbul. Combust. **81**, 583–607 (2008)

27. Chakraborty, N., Klein, M., Cant, R.S.: Stretch rate effects on displacement speed in turbulent premixed flame kernels in the thin reaction zones regime. Proc. Combust. Inst. **31**, 1385–1392 (2007)
28. Dunstan, T.D., Jenkins, K.W.: Flame surface density distribution in turbulent flame kernels during the early stages of growth. Proc. Combust. Inst. **32**, 1427–1434 (2009)
29. Dunstan, T.D., Jenkins, K.W.: The effects of hydrogen substitution on turbulent premixed methane-air kernels using direct numerical simulationnt. Int. J. Hydrog. Energy. **34**, 8389–8404 (2009)
30. Chakraborty, N., Klein, M.: Effects of global flame curvature on surface density function transport in turbulent premixed flame kernels in the thin reaction zones regime. Proc. Combust. Inst. **32**, 1435–1443 (2009)
31. Lecocq, G., Richard, S., Colin, O., Vervisch, L.: Hybrid presumed pdf and flame surface density approaches for large-eddy simulation of premixed turbulent combustion. part 2, Early flame development after sparking. Combust. Flame. **158**, 1215–1226 (2011)
32. Colin, O., Truffin, K.: A spark ignition model for large eddy simulation based on an FSD transport equation (ISSIM-LES). Proc. Combust. Inst. **33**, 3097–3104 (2011)
33. Ahmed, I., Swaminathan, N.: Simulation of spherically expanding turbulent premixed flames. Combust. Sci.Technol. **185**, 1509–1540 (2013)
34. Ahmed, I., Swaminathan, N.: 2014, Simulation of turbulent explosion of hydrogen-air mixtures. Int. J. Hydrog. Energy. **39**, 9562–9572 (2014)
35. Ozel Erol, G., Hasslberger, J., Klein, M., Chakraborty, N.: A direct numerical simulation analysis of spherically expanding turbulent flames in fuel droplet-mists for an overall equivalence ratio of unity. Phys. Fluids. **086104**, (2018)
36. Alqallaf, A., Klein, M., Chakraborty, N.: Effects of Lewis number on the evolution of curvature in spherically expanding turbulent premixed flames. Fluids. **4**, 12 (2019). https://doi.org/10.3390/fluids4010012
37. Ozel Erol, G., Hasslberger, J., Klein, M., Chakraborty, N.: A Direct Numerical Simulation investigation of spherically expanding flames propagating in fuel droplet-mists for different droplet diameters and overall equivalence ratios. Combust. Sci. Technol. (2019). https://doi.org/10.1080/00102202.2019.1576649
38. Poinsot, T.J., Echekki, T., Mungal, M.G.: A study of the laminar flame tip and implications for premixed turbulent combustion. Combust. Sci. Technol. **81**, 45–73 (1992)
39. Haworth, D.C., Poinsot, T.J.: Numerical simulations of Lewis number effects in turbulent premixed flames. J. Fluid Mech. **244**, 405–436 (1992)
40. Rutland, C., Trouvé, A.: Direct Simulations of premixed turbulent flames with nonunity Lewis numbers. Combust. Flame. **94**, 41–57 (1993)
41. Fries, D., Ochs, B.A., Saha, A., Ranjan, D., Menon, S.: Flame speed characteristics of turbulent expanding flames in a rectangular channel. Combust. Flame. **199**, 1–13 (2018)
42. Sahafzadeh, M., Dworkin, S.B., Kostiuk, L.W.: Predicting the reneou of a premixed flame subjected to unsteady stretch rates. Combust. Flame. **196**, 237–248 (2018)
43. Echekki, T., Chen, J.H.: Unsteady Strain rate and curvature effects in turbulent premixed methane-air flames. Combust. Flame. **106**, 184–202 (1996)
44. Chen, J.H., Im, H.G.: Correlation of flame speed with stretch in turbulent premixed methane/air flame. Proc. Combust. Inst. **27**, 819–826 (1998)
45. Echekki, T., Chen, J.H.: Analysis of the Contribution of Curvature to Premixed Flame Propagation. Combust. Flame. **108**, 308–311 (1999)
46. Chakraborty, N., Cant, S.: Unsteady effects of strain rate and curvature on turbulent premixed flames in an inlet-outlet configuration. Combust. Flame. **137**, 129–147 (2004)
47. Chakraborty, N., Cant, R.S.: Influence of Lewis Number on curvature effects in turbulent premixed flame propagation in the thin reaction zones regime, Phys. Fluids. **17**, 105105 (2005)
48. Hawkes, E.R., Chen, J.H.: Direct numerical simulation of hydrogen-enriched lean premixed methane air flames. Combust. Flame. **138**, 242–258 (2004)
49. Hawkes, E.R., Chen, J.H.: Evaluation of models for flame stretch due to curvature in the thin reaction zones regime. Proc. Combust. Inst. **30**, 647–655 (2005)
50. Chakraborty, N.: Comparison of displacement speed statistics of turbulent premixed flames in the regimes representing combustion in corrugated flamelets and thin reaction zones. Phys. Fluids. **19**, 105109 (2007)
51. Chakraborty, N., Hawkes, E.R., Chen, J.H., Cant, R.S.: Effects of strain rate and curvature on Surface Density Function transport in turbulent premixed CH_4-air and H_2-air flames, A comparative study. Combust. Flame. **154**, 259–280 (2008)
52. Han, I., Huh, K.Y.: Roles of displacement speed on evolution of flame surface density for different turbulent intensities and Lewis numbers in turbulent premixed combustion. Combust. Flame. **152**, 194–205 (2008)
53. Mizutani, Y., Nishimoto, T.: Combustion of fuel vapor-drop-air systems: Part II-spherical flames in a vessel. Combust. Flame. **20**, 351–357 (1973)

54. Polymeropoulos, C.E.: Flame propagation in aerosols of fuel droplets, fuel vapor and air. Combust. Sci. Technol. **40**, 217–232 (1984)
55. Silverman, I., Greenberg, J.B., Tambour, Y.: Stoichiometry and polydisperse effects in premixed spray flames. Combust. Flame. **93**, 97–118 (1993)
56. Greenberg, J.B., Silverman, I., Tambour, Y.: On droplet enhancement of the burning velocity of laminar premixed spray flames. Combust. Flame. **113**, 271–273 (1998)
57. Burgoyne, J.H., Cohen, L.: The effect of drop size on flame propagation in liquid aerosols. Proc. R. Soc. London. Ser. A. **225**, 375–392 (1954)
58. Szekely, G.A., Faeth, G.M.: Effects of envelope flames on drop gasification rates in turbulent diffusion flames. Combust. Flame. **49**, 255–259 (1983)
59. Ballal, D.R., Lefebvre, A.H.: Flame propagation in heterogeneous mixtures of fuel droplets, fuel vapor and air. Symp. Combust. **18**, 321–328 (1981)
60. Reveillon, J., Vervisch, L.: Spray vaporization in nonpremixed turbulent combustion modeling: a single droplet model. Combust. Flame. **121**, 75–90 (2000)
61. Nakamura, M., Akamatsu, F., Kurose, R., Katsuki, M.: Combustion mechanism of liquid fuel spray in a gaseous flame. Phys. Fluids. **17**(1–14), (2005)
62. Watanabe, H., Kurose, R., Hwang, S.M., Akamatsu, F.: Characteristics of flamelets in spray flames formed in a laminar counterflow. Combust. Flame. **148**, 234–248 (2007)
63. Reveillon, J., Demoulin, F.X.: Evaporating droplets in turbulent reacting flows. Proc. Combust. Inst. **31**, 2319–2326 (2007)
64. Sreedhara, S., Huh, K.Y.: Conditional statistics of nonreacting and reacting sprays in turbulent flows by direct numerical simulation. Proc. Combust. Inst. **31 II**, 2335–2342 (2007)
65. Xia, J., Luo, K.H.: Direct numerical simulation of inert droplet effects on scalar dissipation rate in turbulent reacting and non-reacting shear layers. Flow, Turbul. Combust. **84**, 397–422 (2010)
66. Fujita, A., Watanabe, H., Kurose, R., Komori, S.: Two-dimensional direct numerical simulation of spray flames - Part 1: Effects of equivalence ratio, fuel droplet size and radiation, and validity of flamelet model. Fuel. **104**, 515–525 (2013)
67. Wacks, D., Chakraborty, N.: Flame structure and propagation in turbulent flame-droplet interaction: A Direct Numerical Simulation analysis. Flow, Turbul. Combust. **96**, 1053–1081 (2016)
68. Wacks, D., Chakraborty, N.: Flow topology and alignments of scalar gradients and vorticity in turbulent spray flames: A Direct Numerical Simulation analysis. Fuel. **184**, 922–947 (2016)
69. Wacks, D., Chakraborty, N., Mastorakos, E.: Statistical analysis of turbulent flame-droplet interaction: A Direct Numerical Simulation study. Flow, Turbul. Combust. **96**, 573–607 (2016)
70. Wang, Y., Rutland, C.J.: Effects of temperature and equivalence ratio on the ignition of n-heptane fuel spray in turbulent flow. Proc. Combust. Inst. **30**, 893–900 (2005)
71. Schroll, P., Wandel, A.P., Cant, R.S., Mastorakos, E.: Direct numerical simulations of autoignition in turbulent two-phase flows. Proc. Combust. Inst. **32**, 2275–2282 (2009)
72. Wandel, A.P., Chakraborty, N., Mastorakos, E.: Direct numerical simulations of turbulent flame expansion in fine sprays. Proc. Combust. Inst. **32**, 2283–2290 (2009)
73. Wandel, A.P.: Influence of scalar dissipation on flame success in turbulent sprays with spark ignition. Combust. Flame. **161**, 2579–2600 (2014)
74. Neophytou, A., Mastorakos, E., Cant, R.S.: The internal structure of igniting turbulent sprays as revealed by complex chemistry DNS. Combust. Flame. **159**, 641–664 (2012)
75. Neophytou, A., Mastorakos, E., Cant, R.S.: DNS of spark ignition and edge flame propagation in turbulent droplet-laden mixing layers. Combust. Flame. **157**, 1071–1086 (2010)
76. Tarrazo, E.F., Sánchez, A.L., Liñán, A., Williams, F.A.: A simple one-step chemistry model for partially premixed hydrocarbon combustion. Combust. Flame. **147**, 32–38 (2006)
77. Malkeson, S.P., Chakraborty, N.: Statistical analysis of displacement speed in turbulent stratified flames: A direct numerical simulation study. Combust. Sci. Technol. **182**, 1841–1883 (2010)
78. Swaminathan, N., Bray, K.N.C.: Turbulent Premixed Flames, p. 5. Cambridge University Press, NewYork (2011)
79. Kumar, K., Freeh, J.E., Sung, C.J., Huang, Y.: Laminar flame speeds of preheated iso-octance/O2/N2 and n-heptane/O2/N2 mixtures. J. Propuls. Power. **23**, 428–436 (2007)
80. Chaos, M., Kazakov, A., Zhao, Z., Dryer, F.L.: A high-temperature chemical kinetic model for primary reference fuels. Int. J. Chem. Kinet. **39**, 399–414 (2007)
81. Chakraborty, N., Cant, R.S.: A-Priori Analysis of the curvature and propagation terms of the Flame Surface Density transport equation for Large Eddy Simulation. Phys. Fluids. **19**, 105101 (2007)
82. Chakraborty, N., Cant, R.S.: Direct Numerical Simulation analysis of the Flame Surface Density transport equation in the context of Large Eddy Simulation. Proc. Combust. Inst. **32**, 1445–1453 (2009)
83. Wray, A.A., Minimal storage time advanced schemes for spectral methods. California (1990)

84. Poinsot, T.J., Lele, S.K.: Boundary conditions for direct simulations of compressible viscous flows. J. Comput. Phys. **101**, 104–129 (1992)
85. Rotexo-Softpredict-Cosilab, GmbH and Co. KG Bad Zwischenahn, Germany
86. Neophytou, A., Mastorakos, E.: Simulations of laminar flame propagation in droplet mists. Combust. Flame. **156**, 1627–1640 (2009)
87. Rogallo, R.S.: Numerical experiments in homogeneous turbulence, California (1981)
88. Peters, N.: Turbulent combustion, Cambridge monograph on mechanics, 1st edn. Cambridge University Press, Cambridge (2000)
89. Grout, R.W.: An age extended progress variable for conditioning reaction rates. Phys. Fluids. **19**, 105107 (2007)
90. Pera, C., Chevillard, S., Reveillon, J.: Effects of residual burnt gas heterogeneity on early flame propagation and on cyclic variability in spark-ignited engines. Combust. Flame. **160**, 1020–1032 (2013)
91. Dopazo, C., Martin, J., Hierro, J.: Local geometry of isoscalar surfaces. Phys. Rev. E. **76**, 056316 (2007)
92. Poinsot, T., Veynante, D.: Theoretical and numerical combustion, 1st Edition, R.T. Edwards Inc, Philadelphia (2001)